

A 8 Density Functional Theory in Practice

Stefan Blügel

Institut für Festkörperforschung

Forschungszentrum Jülich GmbH

Contents

1	Introduction	2
2	Kohn-Sham Approach in a Nutshell	5
2.1	Total Energy and Force	5
2.2	The Kohn-Sham Equations	6
2.3	Magnetism	7
2.4	The Eigenvalue Problem	8
2.5	The CPU Time Requirement	10
2.6	Brillouin-Zone Integration and Fermi Energy	11
2.7	Achieving Self-Consistency	12
3	The Electronic Structure Methods	14
4	Surface Models	16
5	APW-like Concepts to solve the Kohn-Sham Equations	18
5.1	The APW Concept	19
5.2	The LAPW Basisfunctions	21
5.3	The FLAPW-Method in Film Geometry for Surfaces and Thin Films	23
6	The Green function method of Korringa, Kohn and Rostoker	26
6.1	Green Function Method	26
6.2	KKR representation of the Green function	29
6.3	Two-dimensional systems: finite-thickness slabs and half-infinite crystals	31

1 Introduction

Societal requests for environment prediction and protection, the durability of chemicals, the vision of new applications in information technology such as autonomous robots, biondiagnostic systems, or faster information processing, as well as demands on the sustainable and efficient use of resources and energies translate in a huge demand on modeling and simulating properties, chemical reactions, synthesis and growth processes of emergent quantum materials that is based on understanding and is predictive. Modern solid state materials have a multiplicity of novel properties exhibiting for example a rapid (magnetic, ferroelectric, superconducting) phase response to external stimuli such as light, pressure, magnetic field or electrical conductivity, so that manifold uses are possible even today or can be expected for the future. Materials of this sort are often multicomponent systems such as magnetic tunneljunctions (e.g. $\text{NiMnSb|MgO|Co}_2\text{MnSn}$), high-temperature superconductors (e.g. $\text{HgBa}_2\text{Ca}_2\text{Cu}_2\text{O}_8$), or perovskite-type materials with complex magnetic structures.

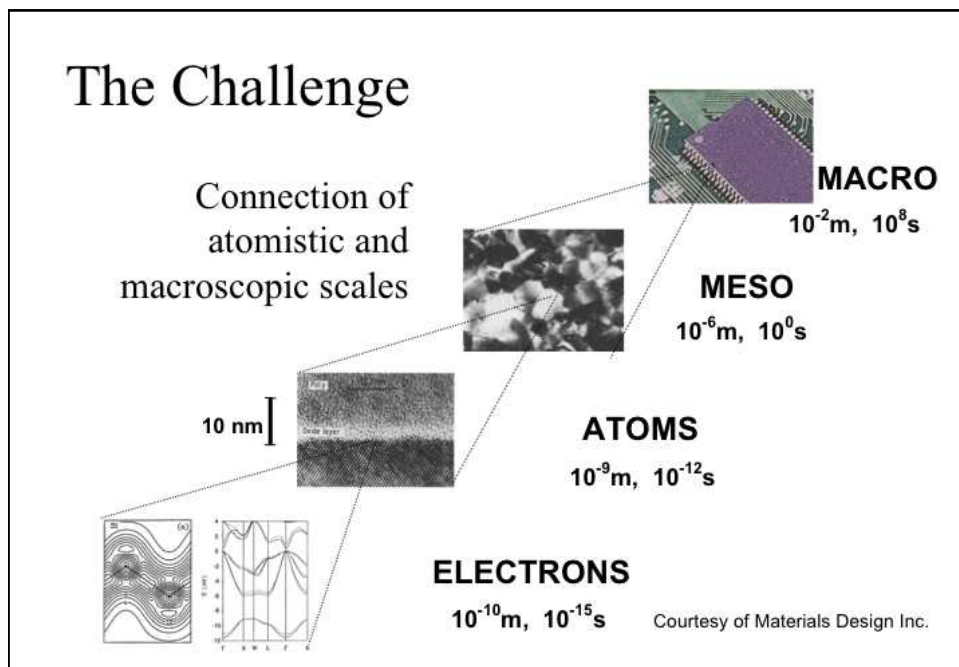


Fig. 1: Although the principles of a MOSFET transistor depends on the electronic properties of doped Si, the functionality, the heat load, the leakage current or the clock speed depend on the quality of interfaces, on the growth and crystallinity of the oxides, the microstructure of the strain and many other factors of very different length scales.

The functionality of macroscopic systems of technological relevance such as for example a chip or a central processing unit (CPU) shown in Fig. 1 depends not only on the distribution of the electrons and their response to external changes on a microscopic scale, but also on the atomic arrangements, the formation of defects, precipitates, inclusions, clusters, interfaces, interface roughness, alloying, textures, and other details of the microstructure taking place on a mesoscopic scale. Thus, the envisaged functionality depends typically on a large number of distinct atomic scale processes, their interdependence and involves a huge number of atoms. This calls for a multiscale modeling, where corresponding theories and their results need to be

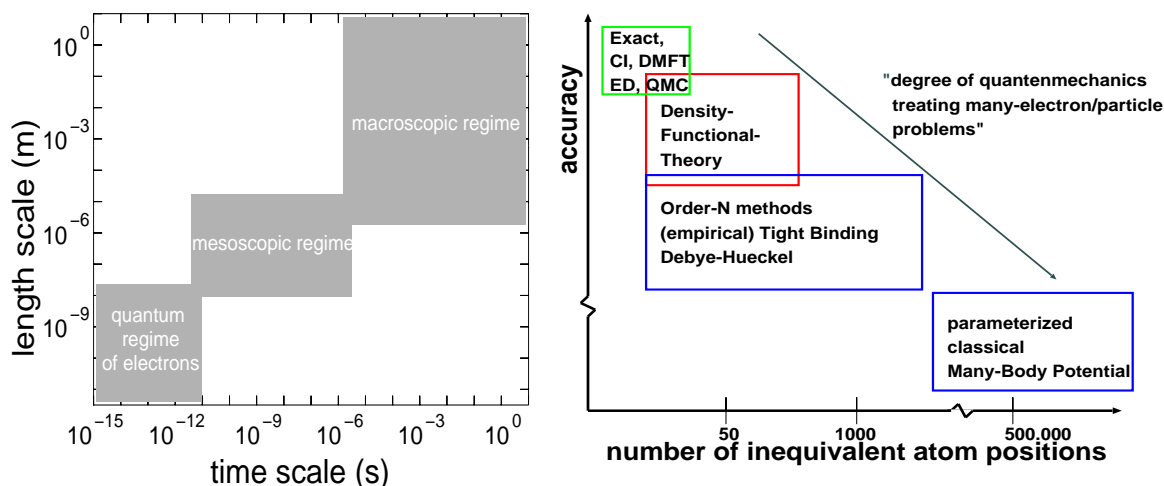


Fig. 2: Left figure: Schematic presentation of the time and length scales relevant for most material science applications. The elementary molecular processes, which rule the behavior of a system, take place in the so-called "quantum regime" governing the dynamics of the electrons. Their interplay are the origin of the functionalities of materials, which develop over meso- and macroscopic length and time scales [1]. Right figure: It is not possible to treat all systems with an equal degree of quantum mechanics. Few electron systems, or models extracted to treat the most relevant interactions of many electrons may be treated with arbitrary accuracy, in general this is not possible. Using density functional theory (DFT) the dynamics of systems with a few hundreds of atoms and 10-20 ps is possible, while large molecular systems with electron gaps between homo- and luma orbitals of a few thousand atoms may be treated with order-N methods. The glass formation, amorphization processes or biological systems involving millions of atoms may be treated with force fields, fitted onto DFT calculations.

linked appropriately. For each regime of length and time scale, the microscopic, mesoscopic and macroscopic one, a number of methodologies are well established and are being developed. Particularly interesting is the boundary where the microscopic regime meets the mesoscopic one, i.e. when laws of quantum mechanics governing the many-electron problem on the microscale meets the statistical physics of the many degrees of freedom of many atoms and spins on the mesoscale. Obviously, then model building becomes important and essential as it is basically impossible and not necessary to treat all degrees of freedom with quantum mechanical accuracy and time scale. On the mesoscale many the time scale and relevance of process are determined by activation barriers, involving processes which need to be treated involving many atoms. One typically deals with rare events, where the time between consecutive events can be orders of magnitude large than the actual event itself. To study this scenario by model building can mean to find the set of relevant processes which are then investigated with microscopic theories, then mapped to classical many-body potential describing a classical force field or a lattice gas model, which is then simulated with a molecular dynamics or an equilibrium or kinetic Monte Carlo method. The evolution of the system at mesoscopic time scale may provide than answers whether the original assumption of relevant elementary processes are consistent with the expected results.

The quest for predictive materials science modeling excludes the use of empirical potentials or fitted force fields on both the microscopic and mesoscopic scale. During the past ten years,

first-principles calculations based on the density-functional theory (DFT) [2] in the local (spin-) density approximation (LDA) or in the generalized gradient approximation (GGA) (for a review see Ref. [3, 4, 5]) emerged as the most powerful framework to respond to the demands mentioned above on a microscopic level. By first-principles (or in Latin: *ab initio*), is meant, that the parameters of the theory are fixed by the basic assumptions and equations of quantum mechanics and, for our discussion, density-functional theory. The overwhelming success of the density-functional theory for the description of the ground-state properties of large material classes including insulators, semiconductors, semimetals, half-metals, simple metals, transition-metals and rare-earths in bulk, at surfaces and as nanostructures makes it the unchallenged foundation of any modern electronic structure theory. The wide applicability combined with the predictive power of the approach turned it to the “standard model” in material science. In principle, the only input needed for the theory are the atomic numbers of the constituent atoms of a system, all other properties follow as a direct consequence of the density-functional equations.

In practice, the definition has to be modified since one is always limited to some set of model systems. These limitations might include system size, crystal structure, neglect of disorder, low or zero temperature, the time-scale or any number of other restrictions on the “phase space” to probe. While some of these restrictions and limitations are burdensome, the goal of calculations is not merely to obtain numbers, but rather insight. By focusing on well-defined, but restricted models, by working on chemical trends rather than on isolated case studies, by investigating systems in hypothetical non-equilibrium structures or follow simulations in idealized environments, which may not be realized in experiments, one is able to develop different levels of understanding of the system in question and may hopefully learn which aspects of the problem are important.

A particularly rich arsenal of assets for material design and tailoring of material properties is provided when the surface of materials is provided as templates for fabrication. Nanostructures down to the atomic scale made of single atoms or of small molecules can be manufactured to form chains and clusters or structures with specific electronic properties by employing the tip of scanning tunneling microscope (STM) or relying on the instruments of self-assembly. Nanostructured thin film systems are decisive functional units in electronic devices, sensors and in biological systems. The existence of particular surface and interface alloys and the complex interplay between morphological, structural, magnetic and electronic features in nanostructured systems stand as examples for a wide field of phenomena which are largely not understood, while offering exceptional technological opportunities at the same time.

The simulation of surfaces provides a good case study for the general aspect of modern materials science. Also here many, may be most, interesting physical phenomena take place at meso- or macroscopic length scales and over times of seconds or even minutes. For example, surface reconstructions sometimes evolve over a time period of seconds or even minutes, and the self-organization of nano-scale structures, such as for example quantum dots, also occurs over macroscopic times. *Ab initio* calculations (electronic structure, total energy calculations as well as molecular dynamics (MD) simulations) are concerned with length scales of a chemical bond and with times determined by interatomic force constants and the corresponding atomic vibrations. To bridge the gap from the atomistic processes to macroscopic dimensions is an important aspect which is covered in this spring school.

In this chapter we aim at discussing the nitty-gritty details of *ab initio* calculations, the interplay of the choice of the electronic structure methods, the structural models, the chemical nature of the participating elements and the microscopic processes in question for the particular example of surface science. The results of such density functional theory (DFT) calculations provide

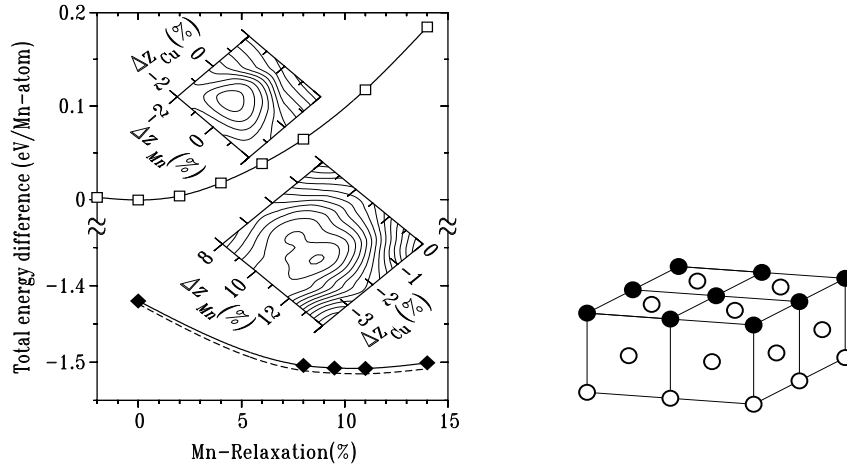


Fig. 3: Example: structural optimization of Mn and Cu surface atoms in a $\text{Cu}(100)c(2 \times 2)\text{Mn}$ surface alloy. Right figure: Schematic representation of the substitutional surface alloy film of one monolayer thickness (\bullet indicates the Mn atoms) grown as overlayer on a fcc (001) substrate (\circ). Left figure: Total energy per Mn atom vs. the buckling relaxation Δz_{Mn} of Mn in relative units with respect to the theoretical interlayer spacing of Cu, $d_{Cu} = 1.76 \text{ \AA}$. The open squares represent the nonmagnetic and the solid diamonds the ferromagnetic results. The solid lines (for Cu atoms fixed at the ideally terminated positions $\Delta z_{Cu} = 0$) and dashed line (the top Cu atom is always at its optimally relaxed position) are the fitting polynomials. The upper (lower) inset shows the contour plot of the nonmagnetic (ferromagnetic) total energy with respect to the buckling of Mn and Cu. The minimum, which determines the optimal structure is found in the inner circle. The contour interval is 1 meV. The energy of the nonmagnetic solution at 0% relaxation was chosen as the origin of the total energy scale (taken from Ref. [6]).

then, for example, detailed input to the kinetic Monte Carlo (KMC) method with which one is able to cope with the issue of crystal growth and the evolution of meso- and macroscopic kinetic growth shapes, which may differ significantly from equilibrium shapes as determined by the minimum of the free energy.

This chapter starts with a quick overview to the Kohn-Sham ansatz outlining the general aspects of the first-principles methodology followed by an introduction to the relevant choice of the geometrical models to simulate surfaces, and the choice of the appropriate electronic structure method. As an example, two electronic structure methods are introduced at a greater depth, which are the full-potential linearized augmented plane wave (FLAPW)-like methods to solve the Kohn-Sham equation for a periodic solid and surfaces, and the Korringa, Kohn and Rostocker (KKR) Green-function method as an example of a Green-function method to cope with the surface geometry.

2 Kohn-Sham Approach in a Nutshell

2.1 Total Energy and Force

In the density-functional theory, the total energy $E[\{\mathbf{R}\}, \{\psi_i\}]$ of a system of interacting atoms and electrons is a functional of the atomic positions $\{\mathbf{R}\}$ and the electron density $n(\mathbf{r})$. The

electron density can be expressed in terms of M occupied single-particle orbitals $\psi_i(\mathbf{r})$:

$$n(\mathbf{r}) = \sum_{i(occ)}^M |\psi_i(\mathbf{r})|^2, \quad (1)$$

where i labels the states. If the total energy functional $E[\{\mathbf{R}\}, \{\psi_i\}]$ is minimized with respect to the electronic degrees of freedom $\{\psi_i\}$, we recover the Born-Oppenheimer surface $\Phi[\{\mathbf{R}\}]$:

$$\Phi[\{\mathbf{R}\}] = \min_{\{\psi_i\}} E[\{\mathbf{R}\}, \{\psi_i\}], \quad (2)$$

on which the atoms move. The derivative of $\Phi[\{\mathbf{R}\}]$ with respect to the atomic position \mathbf{R}^μ gives the force \mathbf{F}^μ ,

$$\mathbf{F}^\mu = -\nabla_{\mathbf{R}^\mu} \Phi[\{\mathbf{R}\}] \quad (3)$$

exerted on the atom μ , which ties electronic structure to structural optimization and molecular dynamics calculations. The energy functional is divided into several terms:

$$E[\{\mathbf{R}\}, \{\psi_i\}] = E_{kin}[\{\psi_i\}] + E_H[\{\psi_i\}] + E_{xc}[\{\psi_i\}] + E_{ext}[\{\mathbf{R}\}, \{\psi_i\}] + E_{ion}[\{\mathbf{R}\}], \quad (4)$$

where E_{kin} is the kinetic energy of non-interacting electrons, E_H is the Hartree energy, i.e. the classical Coulomb energy of the electrons, and E_{xc} is the exchange-correlation energy which contains terms coming from the Pauli principle (exchange hole), from correlations due to the repulsive Coulombic electron-electron interaction and from the contribution to the kinetic energy of interacting electrons [4]. E.g. In the local density approximation $E_{xc}[n]$ is written in the form $E_{xc}[n] = \int d\mathbf{r} n(\mathbf{r}) \varepsilon_{xc}(n(\mathbf{r}))$. Then, E_{ext} is the interaction energy of the electrons with the ions, e.g. described by the $1/r$ potential as in all-electron methods or by pseudo-potentials, and E_{ion} is the classical Coulomb energy of the ions.

2.2 The Kohn-Sham Equations

The single-particle wavefunctions $\psi_i(\mathbf{r})$ are obtained by minimization of the total energy with respect to the wavefunctions subject to the normalization constraint

$$\int d\mathbf{r} |\psi_i(\mathbf{r})|^2 = 1. \quad (5)$$

This leads to the Kohn-Sham equations[7], an eigenvalue problem for the eigenfunctions $\psi_i(\mathbf{r})$ and the eigenvalues ε_i :

$$\hat{H}[n] \psi_i[n] = \varepsilon_i[n] \psi_i[n], \quad (6)$$

where all quantities depend on the electron density n . According to the form of the total energy Eq.(4), the Hamiltonian \hat{H} is a sum of corresponding terms and the eigenvalue problem is written in the form:

$$(\hat{T}_0 + \hat{V}_{ext} + \hat{V}_H + \hat{V}_{xc}) \psi_i(\mathbf{r}) = \varepsilon_i \psi_i(\mathbf{r}) \quad (7)$$

In the real space representation the individual terms are the following:

$$\text{kinetic energy :} \quad \hat{T}_0 = -\frac{\hbar^2}{2m} \Delta_{\mathbf{r}} \quad (8)$$

$$\text{external-potential :} \quad V_{\text{ext}}(\{\mathbf{R}\}, \mathbf{r}) = \sum_{\mu} \frac{e^2 Z^{\mu}}{|\mathbf{r} - \mathbf{R}^{\mu}|} \quad (9)$$

$$\text{Hartree potential :} \quad \Delta_{\mathbf{r}} V_H(\mathbf{r}) = 4\pi e^2 n(\mathbf{r}) \quad (10)$$

$$\text{xc-potential (LDA) :} \quad V_{\text{xc}}(\mathbf{r}) = \frac{\delta}{\delta n(\mathbf{r})} \int d\mathbf{r} n(\mathbf{r}) \varepsilon_{\text{xc}}(n(\mathbf{r})) \quad (11)$$

In a pseudo-potential approach \hat{V}_{ext} is replaced for each atom μ by a pseudo-potential \hat{V}_{ps} . The terms $\hat{V}_H[n]$ and $\hat{V}_{\text{xc}}[n]$ are local potentials and explicitly density dependent. Thus, the Hamiltonian $\hat{H}[n]$ and the wavefunctions $\psi_i([n], \mathbf{r})$ are also dependent on the electron density $n(\mathbf{r})$. Together with the expression Eq.(1) a self-consistency problem to obtain the charge density $n(\mathbf{r})$ is established, which is solved iteratively until the input density (used to define the potential terms in the Hamiltonian) is equal to the output density within the required accuracy. The number of self-consistency iterations N_{iter} is considerably reduced applying Quasi-Newton methods [8].

The external potential $\hat{V}_{\text{ext}}[\{\mathbf{R}\}]$ depends explicitly on the positions $\{\mathbf{R}\}$ of all atoms, which change at certain steps to optimize the atomic structure or every time-step of a molecular dynamics algorithm. Thus, the Hamiltonian $\hat{H}[\{\mathbf{R}\}]$ and the wavefunctions $\psi_i(\{\mathbf{R}\}, r)$ are also dependent on the atomic positions $\{\mathbf{R}\}$. After the self-consistency condition for the electron density has been fulfilled, the atom positions are moved by a molecular static or molecular dynamics time-step, $\{\mathbf{R}(t)\} \rightarrow \{\mathbf{R}(t + \Delta t)\}$. Thus, for N_{MD} molecular time steps the eigenvalue problem has to be solved $N_{\text{MD}} N_{\text{iter}}$ times. These arguments suggest a particular loop structure of a typical first-principles method and a particular sequence how the different elements are calculated. This is summarized in Fig. 4.

Typical codes use LDA exchange correlation potentials and energies of Hedin and Lundqvist[9] or Vosko, Wilk, and Nusair[10], or GGA functionals of Perdew *et al.* [11, 12] are given as analytical expressions of the density and their derivatives in case of the GGA.

2.3 Magnetism

If magnetism occurs, the ground state has a broken symmetry and the ground-state energy is described by functionals which depend on the vector-magnetization density $\mathbf{m}(\mathbf{r})$ as an additional field to the ordinary charge density $n(\mathbf{r})$, discussed so far. An additional term $\mu_B \underline{\sigma} \cdot \mathbf{B}_{\text{xc}}(\mathbf{r})$ appears in the Kohn-Sham equations Eq.(7), where $\mu_B = \frac{e\hbar}{2mc}$ is the Bohr magneton, \mathbf{B}_{xc} is the magnetic xc-field an electron experiences, and $\underline{\sigma}$ are the Pauli spinors. Thus, calculating magnetic systems, one works in a two-dimensional spin-space and the basis functions $\psi_{i\sigma}$ carry an additional spin label $\sigma = \pm 1$. The Hamiltonian is a 2×2 matrix in spin-space and is now hermitian and not symmetric. Complex magnetic structures lower frequently the symmetry of the problem and more states have to be calculated or a much larger fraction of the BZ (cf. Sect.2.6) has to be sampled, respectively, pushing the computational effort to the limits of modern supercomputers. In case of collinear magnetism, e.g. ferro-, ferri-, or antiferromagnetism, $\underline{\sigma} \cdot \mathbf{B}_{\text{xc}}$ reduces to $\sigma_z \cdot B_{\text{xc}}$, the Hamiltonian is diagonal in spin space, the magnetization density m_z is then given by spin-up and -down densities, $m_z(\mathbf{r}) = n_{\uparrow}(\mathbf{r}) - n_{\downarrow}(\mathbf{r})$, and the effort of a magnetic calculation is just twice that of a nonmagnetic one. In general, the magnetic moment

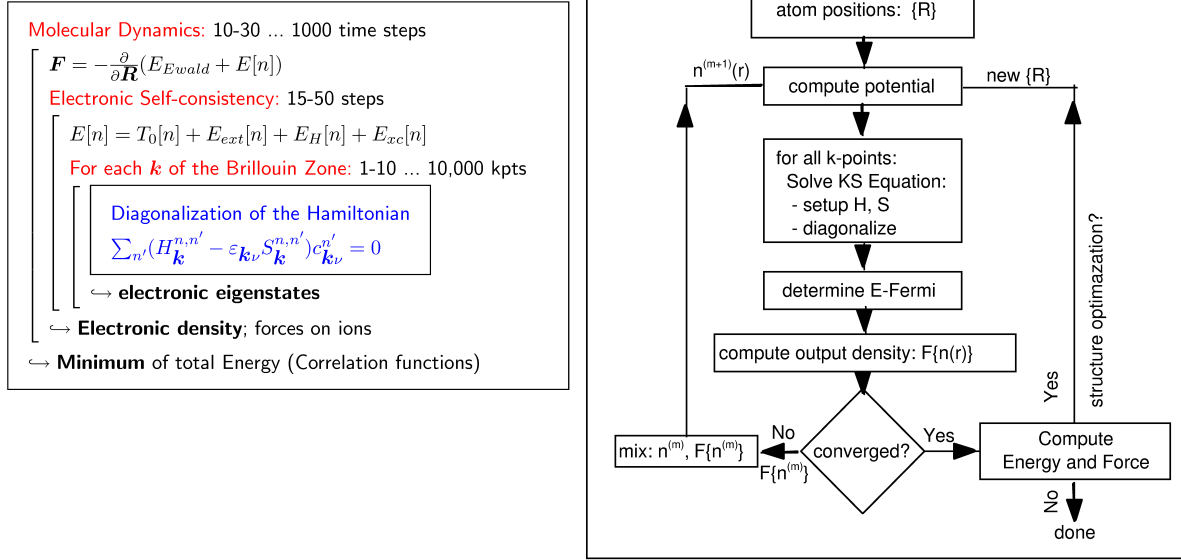


Fig. 4: Right: Typical loop structure of a first-principles code based on density functional theory as applied solid state materials. Left: Schematic flow-chart for self-consistent density-functional calculations e.g. as realized by a FLAPW calculation.

$\mathbf{M} = \int d\mathbf{r} \mathbf{m}(\mathbf{r})$ is a vector quantity, and the search of the magnetic structure can be done dynamically bearing similarities to the dynamical structure optimization combining molecular dynamics and simulated annealing. Therefore, everything said in this chapter on structural optimization applies to both, the atomic and the magnetic structure. Throughout the paper, the spin label is dropped for convenience. More information on the treatment of magnetism can be found in the chapter A.5 “Magnetism in Density Functional Theory” by G. Bihlmayer.

2.4 The Eigenvalue Problem

In all-electron methods eigenvalue problem Eq.(7) is solved for all occupied states i but typically subject to different boundary conditions. As shown schematically in Fig. 5 we distinguish core electrons from valence electrons. The former have eigenenergies which are at least a couple of Rydbergs below the Fermi energy, the potential they experience is to an excellent approximation spherically symmetry and the wavefunctions have no overlap to neighboring atoms. The eigenvalue problem of these states are solved applying the boundary conditions of isolated atoms, which is numerically tackled by a shooting method. Valence electrons in a crystalline solid form electron bands and the eigenvalue problem of is solved subject to the Bloch boundary conditions. The eigenstate is classified by the band index ν and a three-dimensional Bloch vector \mathbf{k} within the first Brillouin zone, ($i \in \{\mathbf{k}\nu\}$). Some materials contain chemical elements with states (e.g. $5p$ states of $4f$ elements or W, p states of early transition metals) intermediate between band and core states and those are coined semi-core states. These are high-lying and extended core states and particular care has to be taken on their treatment since their treatment as core states can cause significant errors in total energy, force and phonon calculations. According to the different treatment of the electrons, we decompose the charge density in the

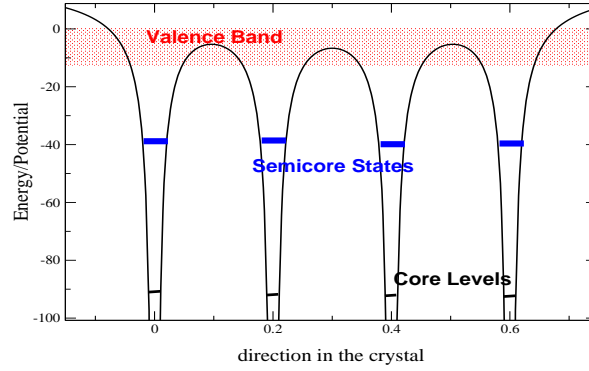


Fig. 5: Schematic representation of the energy position of valence, semi-core and core electrons in periodic potential.

valence, semi-core and core densities

$$n(\mathbf{r}) = n_{\text{val}}(\mathbf{r}) + n_{\text{sc}}(\mathbf{r}) + n_{\text{core}}(r), \quad (12)$$

the latter being spherically symmetric. The charge densities are calculated according to Eq.(1). Wavefunctions and energies of core states give access to hyperfine quantities such as isomer shifts, hyperfine fields and electric field gradient as well as chemical shifts of core levels.

There are many possible ways to solve the Kohn-Sham equations for valence electrons. Frequently, a variational method is chosen by which a wavefunction $\psi_{\mathbf{k}\nu}(\mathbf{r})$ of Bloch vector \mathbf{k} and band index ν is sought as a linear combination of basis functions $\varphi_n(\mathbf{k}, \mathbf{r})$

$$\psi_{\mathbf{k}\nu}(\mathbf{r}) = \sum_{n=1}^N c_{\mathbf{k}\nu}^n \varphi_n(\mathbf{k}, \mathbf{r}) \quad (13)$$

satisfying the Bloch boundary conditions. $c_{\mathbf{k}\nu}^n$ are the expansion coefficients of the wavefunction (coefficient vector), and N is the number of basis functions taken into account. By this expansion, the eigenvalue problem

$$\hat{H}\psi_{\mathbf{k}\nu}(\mathbf{r}) = \varepsilon_{\mathbf{k}\nu}\psi_{\mathbf{k}\nu}(\mathbf{r}) \quad (14)$$

is translated in into an algebraic eigenvalue problem of dimension N

$$(\mathbf{H}(\mathbf{k}) - \varepsilon_{\mathbf{k}\nu}\mathbf{S}(\mathbf{k}))\mathbf{c}_{\mathbf{k}\nu} = 0 \quad \forall \mathbf{k} \in \text{BZ} \quad (15)$$

for the coefficient vector $\mathbf{c}_{\mathbf{k}\nu}^n$ corresponding to the eigenvalues $\varepsilon_{\mathbf{k}\nu}$. The Hamilton $H^{n,n'}(\mathbf{k})$ and overlap matrices $S^{n,n'}(\mathbf{k})$ are hermitian or real symmetric, depending on the point symmetry of the atomic structure. If the basis functions are orthonormal, i.e. $\langle \varphi_n | \varphi_{n'} \rangle = \delta^{n,n'}$, as for example in case of simple planewaves, then the overlap matrix \mathbf{S} , defined as

$$S^{n,n'}(\mathbf{k}) = \int_{\Omega} \varphi_n^*(\mathbf{k}, \mathbf{r}) \varphi_{n'}(\mathbf{k}, \mathbf{r}) d^3r \quad (16)$$

becomes diagonal, $S^{n,n'}(\mathbf{k}) = \delta^{n,n'}$, and the generalized eigenvalue problem Eq.(15) becomes of standard type. Ω is the volume of the unit cell.

In general, the general eigenvalue problem is reduced to a standard one using the Cholesky decomposition. It can be shown (e.g. Stoer [13]), that any hermitian and positive definite matrix can be decomposed into a matrix product of a lower triangular with only positive diagonal elements matrix and its transposed. Clearly, the overlap matrix satisfies these conditions and can be written $S = LL^{tr}$. Therefore, Eq.(15) becomes

$$Hc_i = \varepsilon_i LL^{tr} c_i, \quad (17)$$

multiplying from the left with L^{-1} and introducing a unit matrix we finally find

$$Px_i = \varepsilon_i x_i, \quad (18)$$

after we have P defined as $P = L^{-1}H(L^{-1})^{tr}$ and $x_i = L^{tr}c_i$. Thus, the generalized eigenvalue problem has been reduced to a simple one. The eigenvectors c_i can be obtained by the back-transformation, $c_i = (L^{tr})^{-1}x_i$.

The choice of the most efficient numerical algorithm to solve Eq.(15) depends on the number of basis functions N and the number M of states ν taken into account. If $M/N > \sim 0.1$, direct numerical diagonalization schemes are employed, for example parallelized eigenvalue solver taken from the `ScALAPACK` library package. If $M/N < \sim 0.1$ or if N is too large to fit the eigenvalue problem into the memory of a computer the eigenvalue problem is solved iteratively. Any iterative solution of an eigenvalue problem can be divided into two parts: (i) the determination of the iterative improvement of the state vector $c_{k\nu}^{n,[m]}$ at iteration step m by multiplying the Hamiltonian with the state vector to obtain the update $c_{k\nu}^{n,[m+1]}$:

$$c_{k\nu}^{n,[m+1]} = \sum_{n'} H^{n,n'}(\mathbf{k}) c_{k\nu}^{n',[m]}, \quad (19)$$

and (ii) the orthonormalization of the wave functions

$$\sum_n c_{k\nu}^{n,[m+1]} c_{k\nu'}^{n,[m+1]} = \delta_{\nu,\nu'}. \quad (20)$$

(iii) Frequently, each iteration step is accompanied by a direct sub-space diagonalization of a dimension proportional to M , on which Hamiltonian \hat{H} is projected. If the multiplication of $H \cdot c$ can be made fast by expressing the Hamiltonian in terms of dyadic products or convolutions as in norm-conserving or ultra-soft pseudo-potentials minimizing thereby the number of multiplications, iterative methods become particular beneficial.

2.5 The CPU Time Requirement

The number of basis functions N is determined by the required precision P of a calculation and by the volume Ω of the unit cell or the number of atoms in the unit cell, N_A , respectively. The precision P is controlled by the finest real-space resolution the basis functions can resolve. For three-dimensional unit cells N scales as $N \propto P^3$. In general, the triple (N_k, M, N) , the number of \mathbf{k} -vectors in the BZ used, the number M of states ν considered, and the number of basis functions N are determined by the required precision of the calculation and by the volume of the unit cell. These parameters determine the CPU-time and memory requirements of the calculations. Keeping the loop-structure in mind exhibited in Fig. 4, typically the calculational CPU time scales as

$$\text{CPU} \propto N_{\text{MD}} \cdot N_{\text{iter}} \cdot N_{\mathbf{k}} \begin{cases} N^3 & \text{direct diagonalization} \\ M_{\text{iter}}(MN \ln N + NM^2) & \text{iterative diagonalization} \end{cases} \quad (21)$$

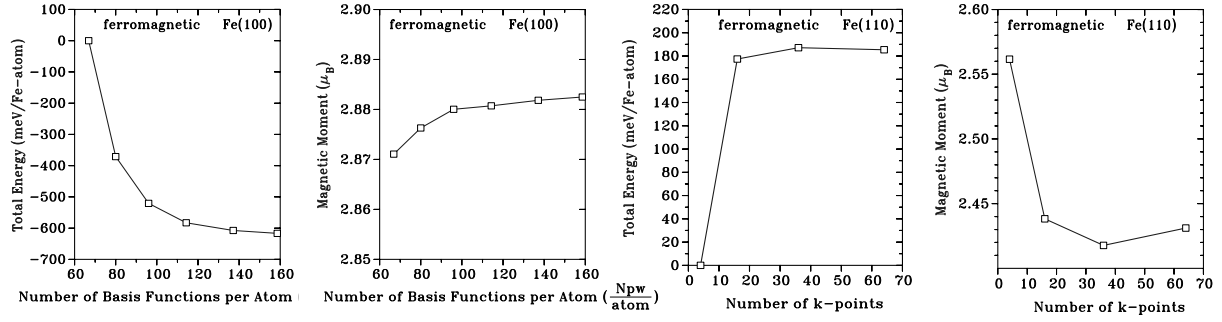


Fig. 6: Test of convergence carried out by the FLAPW method of (absolute) total energy and magnetic moment as function (i) of the number of the LAPW basis functions (see two left figures) for a 7 layer Fe(100) film and (ii) number of special k -points in the IBZ (see two right figures) for an 11 layer Fe(110) film. The calculations of (i) were carried out for the rkm -parameters $rkm = 7.5, 8.0, 8.5, 9.0, 9.5, 10.0$ corresponding to $N = 67, 80, 96, 114, 137, 158$ basis functions.

where M_{iter} gives the number of eigenvalue iterations. This gives just a gross estimate as for iterative methods based on the Car-Parrinello idea where self-consistency iterations and eigenvalue iterations can be combined to directly minimize total energy functional $N_{\text{MD}} \cdot N_{\text{iter}} \cdot M_{\text{iter}}$ depends on many details. The scaling relation for precision scaling is:

$$\text{the number of k-points: } N_k \propto P_k^3 \quad (22)$$

$$\text{the number of basis functions } N: N \propto P^3, \quad (23)$$

where P_k is the precision controlling the k -point summation, e.g. of the force, the total energy or the electron density. Assuming that the volume Ω of the unit cell is proportional to the number of atoms N_A , the scaling relation for volume scaling is:

$$\text{the number of k-points: } N_k \propto 1/N_A, \quad (24)$$

$$\text{the number of states } \nu: M \propto N_A, \quad (25)$$

$$\text{the number of basis functions } N: N \propto N_A, \quad (26)$$

From these considerations it is argued to develop electronic structure methods (cf. Sect. 3) with efficient basis sets to reduce their number N , to develop algorithms to accelerate the convergence (cf. Sect. 2.7) and to employ an efficient k -point integration scheme (cf. Sect. 2.6).

2.6 Brillouin-Zone Integration and Fermi Energy

The calculation of the electron density, total energy, force or stress tensor for infinite periodic solids require the integration of functions over the Brillouin zone that depend on the Bloch vector and the energy band. These integrations stretch only over the occupied part of the band, i.e. over the region of the Brillouin zone where the band energy $\epsilon_\nu(\mathbf{k})$ (ν is the band index) is lower than the Fermi energy. Hence, the integrals are of the form

$$\frac{1}{V_{BZ}} \int_{BZ} \sum_{\nu, \epsilon_\nu(\mathbf{k}) < E_F} f_\nu(\mathbf{k}) d^3k, \quad (27)$$

where f is the function to be integrated, e.g. $f = 1$ for the total number of electrons, $f = \varepsilon$ for the eigenvalue sum and so on. Numerically, these integrations are performed on a discrete mesh in the Brillouin zone. In fact the effort of the BZ integration is in practice significantly reduced by employing the point group symmetry, where the integration is reduced to the irreducible wedge of the BZ (IBZ). There are different methods, that can be used to perform the integration, e.g. the special points method [14, 15] and the tetrahedron method [16, 17, 18]. The special points method is a method to integrate smoothly varying periodic functions of \mathbf{k} . The function to be integrated has to be calculated at a set of special points in the IBZ, each of which is assigned a weight. Thus, the BZ integration is transformed into a sum over a set of \mathbf{k} -points. At each \mathbf{k} -point a sharp energy cut-off is introduced to include only those state in the summation whose energy is below the Fermi energy. Thus, the integrals become:

$$\frac{1}{V_{BZ}} \int_{BZ} \sum_{\nu, \epsilon_\nu(\mathbf{k}) < E_F} f_\nu(\mathbf{k}) d^3k \longrightarrow \sum_{\mathbf{k} \in \text{IBZ}} \sum_{\nu, \epsilon_\nu(\mathbf{k}) < E_F} f_\nu(\mathbf{k}) w(\mathbf{k}) \quad (28)$$

Alternatively, this integration can be viewed as an integration over the whole Brillouin zone, where the function to be integrated is given by a product of the function f with a step function that cuts out the region of the Brillouin zone, where the band energy is above the Fermi energy. Clearly, the resulting function does not satisfy the condition of being smoothly varying. Therefore, the special \mathbf{k} -points method does not converge very quickly, and rather many \mathbf{k} -points are needed to obtain accurate results. On the other hand this method is simple to implement, because the weights depend only on \mathbf{k} and the band energy (via the step function) at each \mathbf{k} -point. Another problem arises from this “sharp” differentiation between occupied and empty bands (parts of bands). Let’s consider a band that is very close to the Fermi energy at a certain \mathbf{k} -point. During the iterations the energy of this band might rise above or drop below the Fermi energy. This leads to sudden changes in the charge density, which can slow down or even prevent the convergence of the density. These sudden changes are clearly a result of the discretization in momentum space. To avoid this problem, the sharp edges of the step function are smoothened, e.g. by introducing a so-called temperature broadening in the context of a the Fermi function $(e^{(\epsilon - E_F)/k_B T} + 1)^{-1}$ rather than the step function. The temperature T or energy Tk_B are an additional external parameters adjusted to obtain the best convergence.

2.7 Achieving Self-Consistency

According to Sect. 2.2 the Kohn-Sham equation Eq.(7) are Schrödinger-like independent-particle equations which must be solved subject to the condition that the effective potential field $V_{\text{eff}}(\mathbf{r}) = V_{\text{ext}}(\mathbf{r}) + V_H(\mathbf{r}) + V_{\text{xc}}(\mathbf{r})$ and the density field $n(\mathbf{r})$ are consistent. The electron density $n_0(\mathbf{r})$ that minimizes the energy functional is a fix-point of the mapping

$$n'(\mathbf{r}) = F\{n(\mathbf{r})\}. \quad (29)$$

i.e. it solves

$$\mathcal{F}\{n_0(\mathbf{r})\} = 0, \quad \text{with } \mathcal{F}\{n(\mathbf{r})\} = F\{n(\mathbf{r})\} - n(\mathbf{r}). \quad (30)$$

(The same can be formulated for the potential.) Typically, the density is expanded into a large set of basis functions. Thus, in actual calculations, the charge density is a coefficient vector of dimension $N_Q \sim 8 * N$ (N defined as in Eq.(13) and Eq.(30) constitutes a system of N_Q nonlinear equations, which can be solved by iteration:

$$n^{m+1}(\mathbf{r}) = F\{n^m(\mathbf{r})\}. \quad (31)$$

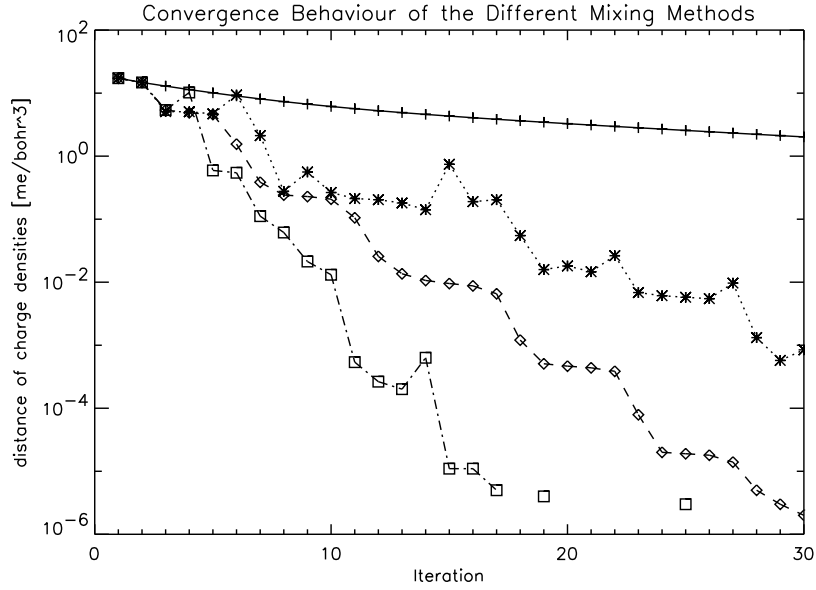


Fig. 7: Comparison of the convergence of charge density calculated by different methods for a non-magnetic bcc Fe crystal using the FLAPW method. Calculations are carried out for mixing parameter $\alpha = 0.04$. + corresponds to simple mixing, and different Quasi-Newton methods: * Broyden's 1st method, \diamond Broyden's 2nd method, \square generalized Anderson method. The distance of the residual vector vs. number of iterations is plotted semi-logarithmically [19].

A starting density $n^{(0)}(\mathbf{r})$ can be constructed by a superposition of atomic densities. A straight mapping as is suggested in Eq.(31) is in general divergent. Convergence can be achieved if the output density $F\{n^m(\mathbf{r})\}$ is mixed with the input density $n^m(\mathbf{r})$.

The simplest and slowest of such mixing schemes is the so-called “simple mixing”, which converges only linearly. The density for the next iteration is constructed as a linear combination of $n^{(m)}$ and $F\{n^m\}$ according to:

$$n^{(m+1)} = (1 - \alpha)n^{(m)} + \alpha F\{n^m\} = n^{(m)} + \alpha \mathcal{F}\{n^{(m)}\}, \quad (32)$$

where α is the so-called mixing parameter. If it is chosen small enough, the iteration converges and is very stable. However, for the type of systems one is interested in, α is very small, requiring many hundreds of iterations. In spin-polarized calculations different mixing parameters can be used for the charge and the magnetization density. Usually, the spin mixing parameter can be chosen far larger than the parameter for the charge density.

In the Newton-Raphson method, the functional $\mathcal{F}\{n\}$ is linearized around the approximate solution $n^{(m)}$.

$$\mathcal{F}\{n\} \approx \mathcal{F}\{n^{(m)}\} + \mathcal{J}\{n^{(m)}\}(n - n^{(m)}), \quad \mathcal{J}\{n^{(m)}(\mathbf{r})\} = \left. \frac{\partial \mathcal{F}\{n(\mathbf{r})\}}{\partial n(\mathbf{r}')} \right|_{n^{(m)}(\mathbf{r})}. \quad (33)$$

In actual calculations the Jacobian \mathcal{J} is a $N_Q \times N_Q$ matrix. Similar to the well-known Newton method to find zeros of one-dimensional functions, the next approximation to n_0 , $n^{(m+1)}$, is determined from the requirement, that the linearized functional in Eq.(33) vanishes at $n^{(m+1)}$. Thus, $n^{(m+1)}$ is given by:

$$n^{(m+1)} = n^{(m)} - [\mathcal{J}\{n^{(m)}\}]^{-1} \mathcal{F}\{n^{(m)}\}. \quad (34)$$

In opposite to the simple mixing, the Newton-Raphson method converges quadratically. The major drawback of this method is the difficulty to evaluate the Jacobian. Even if the functional $\mathcal{F}\{n\}$ were known, the evaluation would be cumbersome due to the enormous size of $\mathcal{J}\{n\}$. In addition, the Jacobian has to be inverted where the amount of calculation scales with cube of the dimension. A further problem is that the convergence radius is rather small so that the method can only be used if $n^{(m)}$ is already very close to n_0 .

The development of the Quasi-Newton methods made it possible to exploit the advantages of the Newton-Raphson method, i.e. to make use of the information that is contained in the Jacobian, for problems where the Jacobian cannot be calculated or its determination is too demanding. Rather than computing the Jacobian each iteration, an approximate Jacobian is set up and improved iteration by iteration. From the linearization of $\mathcal{F}\{n\}$ in Eq.(33) we find the following condition for the Jacobian, which is usually called Quasi-Newton condition:

$$\Delta n^{(m)} = [\mathcal{J}^{(m)}]^{-1} \Delta \mathcal{F}^{(m)} \quad (35)$$

$$\Delta n^{(m)} = n^{(m)} - n^{(m-1)}, \quad \Delta \mathcal{F}^{(m)} = \mathcal{F}\{n^{(m)}\} - \mathcal{F}\{n^{(m-1)}\}$$

Quasi-Newton methods converge super-linearly and have a larger convergence radius than the Newton-Raphson method. Since the Jacobian is build up iteration by iteration, the “history” of the previous iterations is memorized in \mathcal{J} , whereas the Jacobian of the Newton-Raphson method depends only on the previous iteration. In this sense the Newton-Raphson method is self-corrective [53], it “forgets” inadequately chosen corrections. The Quasi-Newton methods sometimes need to be restarted, if the iteration converges only slowly. This can happen if the starting density is very far from n_0 or when physical or numerical parameters that affect the calculations are changed during the iteration. Eq.(35) does not determine the Jacobian uniquely, instead Eq.(35) constitutes a system of N_Q equations for N_Q^2 unknowns. The various Quasi-Newton schemes differ by the ansatz how the new information is used to build the inverse Jacobian. The quality of the convergence is measured by the distance of the residual vector:

$$d_{n^{(m)}} = \|\mathcal{F}\{n^{(m)}\}\| = \|\mathcal{F}\{n^{(m)}\} - n^{(m)}\|. \quad (36)$$

3 The Electronic Structure Methods

The quest to solve the Kohn-Sham equation (7) efficiently for periodic solids, solids with surfaces and interfaces, clusters and molecules has lead to a wide spectrum of very successful and efficient electronic structure methods. Treating isolated clusters or molecules, methods based on localized orbitals are frequently selected going hand in hand with the chemical intuition of a system in question. Considering methods applicable to periodic solids, frequently algorithms are chosen where the Bloch boundary condition can be included in the basis set. Guiding principles to develop electronic structure methods are obtained by having a closer look at the mathematical nature of the Schrödinger-like Kohn-Sham equation Eq.(7) with the kinetic energy operator Δ and the $1/r$ singularity at the nucleus with the simultaneous necessity to calculate the xc-potential $V_{xc}[n](\mathbf{r})$ and the Hartree potential $V_H[n](\mathbf{r})$.

The planewave basis is obviously a very good choice, as the planewave is diagonal to the Laplace operator Δ appearing in both the the kinetic energy operator and in the Poisson equation to calculate the Hartree potential (cf. Eq.(8)), and for a function expanded in planewaves, its power is also completely expressible by a planewave expansion. This property is needed for

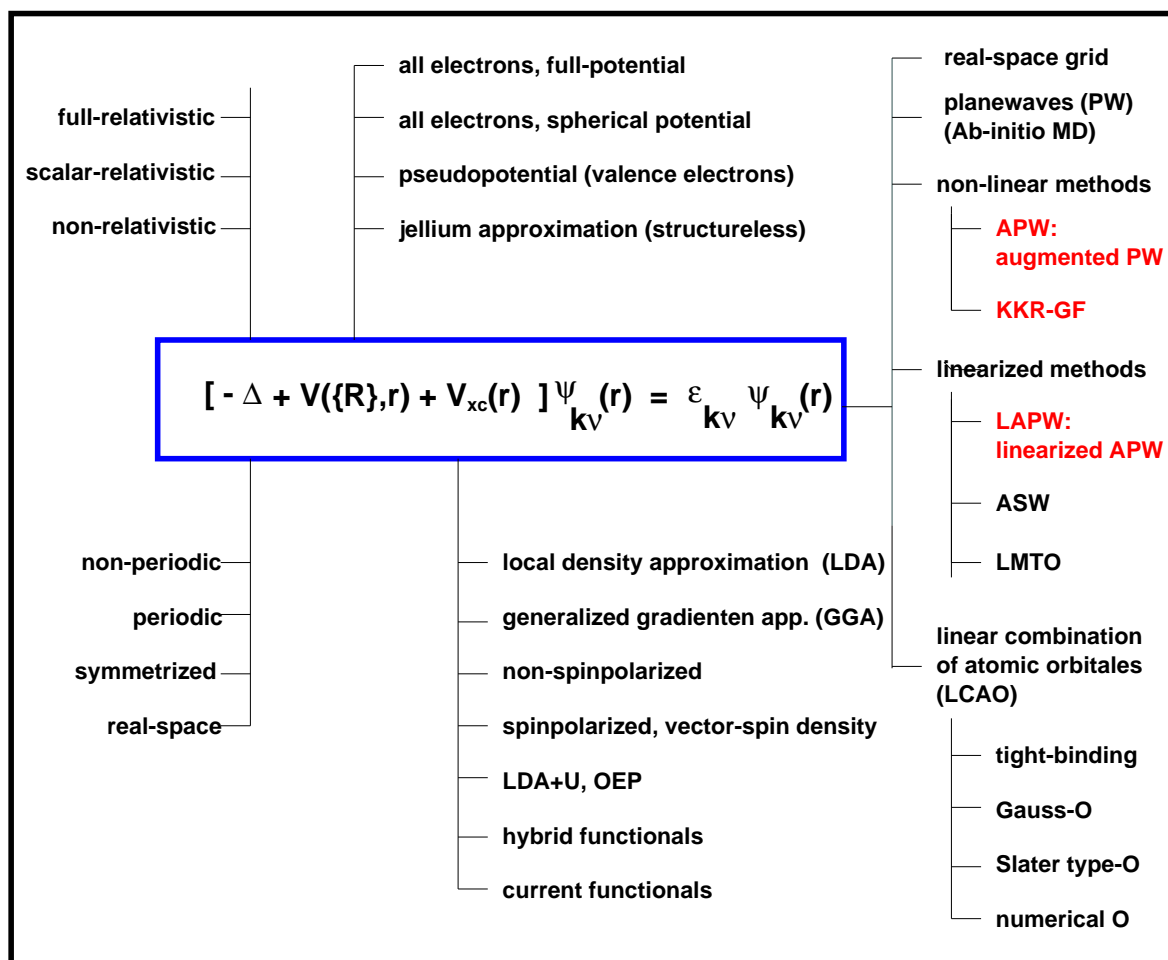


Fig. 8: Very rough and schematic overview of electronic structure methods indicating a rich spectrum of methods developed for different purposes, applications, geometries and symmetries, chemical elements and materials requiring different approximations.

calculating the charge density from the wave function. Thus, using a planewave basis set the calculation of the kinetic energy, charge density and the Hartree potential are obtained by simple algebraic expressions. The calculation of the $V_{xc}(\mathbf{r})$ best performed if the charge density is expressed in real-space. The discrete fast Fourier transformation (FFT) provides a fast algorithm to communicate between both spaces. However, planewave basis sets do not converge at the presence of the $1/r$ singularity. Thus, planewave basis-sets can only be used in the context of a pseudopotential approximation to the true potential where the $1/r$ potential has been replaced by an appropriate smooth potential (For details see chapter A.8 of K. Schroeder: Car-Parrinello Molecular Dynamics and Reaction Kinetics).

All-electron methods have to cope with the $1/r$ singularity. Since this singularity cannot be dealt with variationally, one typically works here with basis functions, which are the numerical solution of $(-\Delta + V_{\text{eff}} - E_l)\varphi = 0$ of the effective (spherical) potential containing the $1/r$ singularity, computed in a sphere around the atom at a given energy parameter E_l . These basis functions treat the singularity exactly. The matching of this wavefunction in such a sphere to the rest of the crystal outside the sphere divides the all-electron methods with regard to the eigenvalue dependence of the basis set into two groups: The nonlinear methods as for example

the Korringa, Kohn and Rostocker (KKR) method and the APW method, and the linear methods, of which the most commonly used are the linear muffin-tin orbital method (LMTO) [20] (see also chapter A.12 of E. Pavarini: Building Model Hamiltonians for Strongly Correlated Materials), the augmented spherical [21] and the APW-based schemes, e.g. FLAPW method.

The choice of the electronic structure method for surface science application, depends on the chemical elements involved, the symmetry of the system and depends on the physical and chemical questions to be answered, and as such also on the relevant geometrical model to treat a surface. Surfaces provide open structures and a correct treatment of the shape of the charge density, the one-electron potential is required. This is offered by so-called full-potential methods such as the PP-PW, PAW, FLAPW, FPLMTO and KKR methods. *Ab initio* molecular dynamics and transition-state calculations are most efficiently calculated by PP-PW and PAW method. All-electron methods on the other hand offer a precise treatment of $3d$ and $4f$ electrons, magnetism is included rigorously, correlation beyond the local-density approximation enters naturally in those methods and nuclear quantities [22] e.g. isomer shift, hyperfine field, electric field gradient (EFG), and core level shift are calculated routinely. At the end a couple of methods proved powerful to cope with the various demands of surface chemistry and physics.

4 Surface Models

Considering the expense of the calculation and physical problem in mind, one of the most crucial steps in computational science is the creation of relevant geometric models. Many, but by no means all phenomena in surface science are relatively short-range in nature. This makes it possible to choose geometric models which are small enough to be tractable to today's electronic structure methods yet still large enough to be physically meaningful. Systems containing of the order of 100 transition-metal atoms or 300 hundred semiconductor elements of group III, IV, V per unit cell can be treated on a first-principles level with today's programs and computer hardware, of course depending on details of the systems in question. A particular choice depends on the physical and chemical questions to be answered, and each geometric model has its strengths and limitations. In the following, we will discuss the most common geometric models for electronic structure calculations of surfaces (cf. Fig. 9) and outline their range of applicability.

Conceptually the most satisfying surface geometry is that of a semi-infinite solid. This geometry can be used from the simple jellium model of surfaces. In the jellium model, the positive charge of the atomic nuclei is simply represented by a uniform constant positive background inside the solid and zero outside an appropriately chosen surface plane. Effectively, the system is thus reduced to a one-dimensional problem and the distribution of the electrons are then calculated using DFT.

The use of a semi-infinite solid is much more difficult if a full three-dimensional solution of the DFT problem is attempted. However, it is reasonable to assume that any material becomes bulk-like at a certain distance away from the surface. A priori, one does not know that distance, but the electronic screening length is a good measure. This results to about 10 layers underneath the surface for transition metals and semiconductors and about 20 layers for sp-metals such as Al, Bi or Pb. In the top layers or the so-called "surface region", the electronic wave functions are then chosen to match the bulk states inside the solid and satisfy the vacuum boundary conditions above the surface. Green function techniques are used, for example, in the Korringa, Kohn and Rostocker (KKR) or in the Full-Potential Linearized Augmented (FLAPW) Green

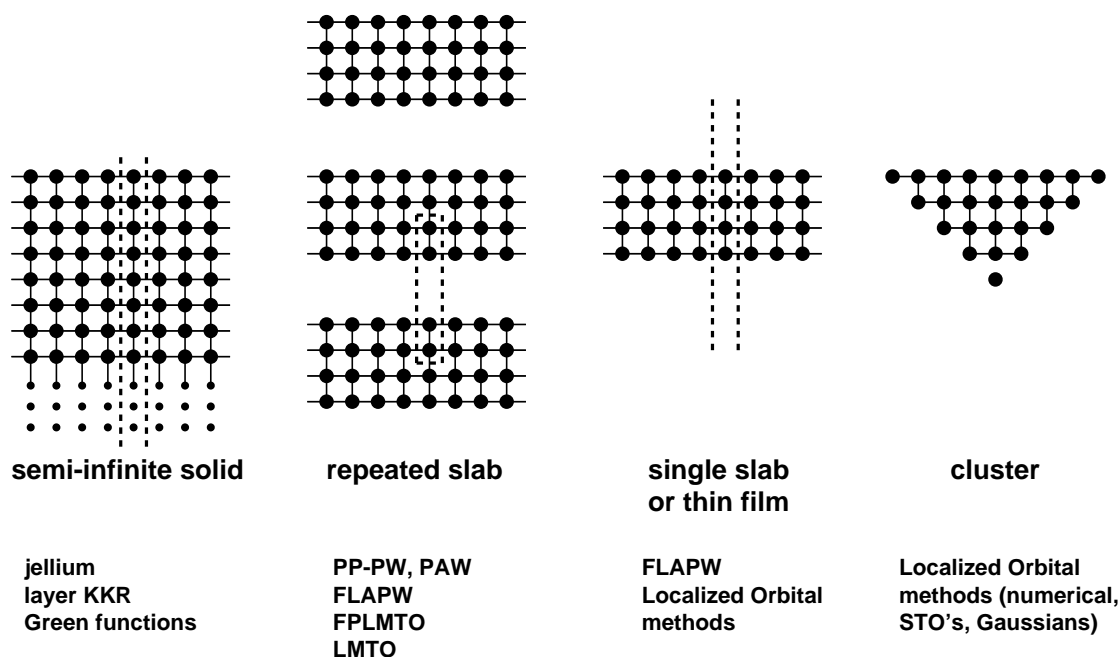


Fig. 9: Geometric models for practical surface calculations. The geometry of a semi-infinite solid is mainly used for jellium calculations and methods employing Green functions and matching techniques. Standard band structure methods using three-dimensional periodicity can be directly applied to a repeated slab geometry. These standard methods include the pseudopotential plane-wave methods (PP-PW), the projector augmented plane wave method (PAW), the full-potential linearized augmented planewave (FLAPW) method, the full-potential linearized muffin-tin orbital (FPLMTO) and the LMT0 method. Much CPU time can be saved using the single slab geometry, which treats the semi-infinite surface on both sides of the slab accurately. The FLAPW method has been implemented for the single slab geometry, which also can be used with localized orbital methods. The cluster geometry is amenable for localized orbital methods with numerical functions, Slater type orbitals (STO's) or Gaussian as basis set, as used for molecular quantum chemical calculations [23].

function methods [24, 25], which provide the necessary mathematical apparatus to accomplish this matching procedure [26].

A simple, but effective geometric surface model is the repeated slab geometry (cf. Fig. 9) calculations of surfaces (cf. Fig. 9). Thin films consisting of about 10 to 20 layers are repeated in the direction perpendicular to the surface. The slabs are chosen thick enough to approach bulk-like behavior near the center of each slab and the spacing is taken large enough so that any artificial interactions across the vacuum region between the slabs are minimized. About 10 to 20 Å are usually sufficient to fulfill the requirement. For such a geometry, any three-dimensional electronic structure method able to treat open structures can be used. The most common approaches for three-dimensional electronic structure calculations are the pseudopotential plane wave (PP-PW) method, the full-potential linearized augmented planewave (FLAPW) method, and the full-potential linearized muffin-tin orbital (FPLMTO) method. Practical applications of these approaches are limited by the number of atoms in the three-dimensional supercell. Thus, a compromise needs to be found between slab thickness, space between the slabs, and the computational effort.

One way to overcome at least one of these limitations is the use of a single-slab geometry (cf. Fig. 9). The slab still has to be thick enough to achieve bulk-like behavior in its interior, but the correct vacuum boundary conditions of the semi-infinite vacuum on both sides of the slab are full-filled. Besides the more accurate description of the vacuum, the surface state and the workfunction, to computational effort may be reduced to 50% of the effort required in an supercell approach of a repeated slab model.

Finally, surface can be modeled by finite clusters. This approach has been widely used for the investigation of chemisorption, since it allows the application of standard quantum chemistry programs. While reasonable structural information such as adsorption geometries can be obtained with relatively small clusters consisting of 10 or 20 atoms, much larger clusters of preferably well over 100 atoms are required to achieve reliable results for sensitive quantities such as adsorption energies or the distinction between different adsorption sites with similar energy. However, even for large clusters, termination effects can have unpredictable side effects.

5 APW-like Concepts to solve the Kohn-Sham Equations

In this section, we introduce step-by-step the full-potential linearized augmented planewave (FLAPW) method [27, 28], to solve the density-functional equations for a crystalline solid and with emphasis for an ultrathin film (a review is given by D. J. Singh [29]). The method originates from the APW method proposed by Slater [30, 31, 32]. Great progress of the APW methodology was achieved as the concept of linear methods [33, 20, 34, 35, 36], was introduced by Andersen and first applied by Koelling and Arbmán using a model potential within the muffin-tin approximation. The linearized APW (LAPW) method reconciled the linear-algebra formulation of the variational problem with the convergence properties of the original formulation and allowed a straight forward extension of the method to the treatment of crystal potentials of general shape. The treatment of the potential and charge density without shape approximation [37, 38] and the implementation of the total energy [28] let to the development of FLAPW bulk [27, 38, 39, 40, 41, 42, 43, 44] film codes [27, 44, 45, 46]. It was during this time that the power and accuracy of the method were demonstrated to the community, largely through a series of calculations of surface and adsorbate electronic structures (for a review see Wimmer *et al.* [47]). These and other demonstrations established the FLAPW method as the method of choice for accurate electronic structure calculations for a broad spectrum of applications.

Constant conceptual and technical developments and refinements such as the proposal and implementation of the scalar-relativistic approximation (SRA) [48], the spin-orbit interaction by second variation [50], and the possibility to calculate forces [51, 52] acting on the ions to carry out structure optimizations, quasi-Newton methods [53] to accelerate the self-consistency iterations, the iterative diagonalization techniques [54, 55, 56], the proposal of a new efficient basis sets, the LAPW+LO [57] and APW+lo [58] basis, in which the APW basis is amended by local orbitals (lo), the extension of the method to non-collinear magnetism [59], to the wire geometry [60], to calculations of the quasiparticle self-energy in the *GW* approximation [61], and the recent formulation and application of the scattering problem in semi-infinite crystals [24, 25, 26] has made APW-like methods, and for our discussion the FLAPW method, a robust, versatile and flexible method, at reasonable computational expense. It is an all-electron method, that means, one works with a true crystal potential, which diverges as $1/r$ at the nucleus, as opposed to the pseudo-potential (for a review see Ref. [62, 63]), in which the singularity is removed. The method and the breadth of applications has benefited from the large growth of available com-

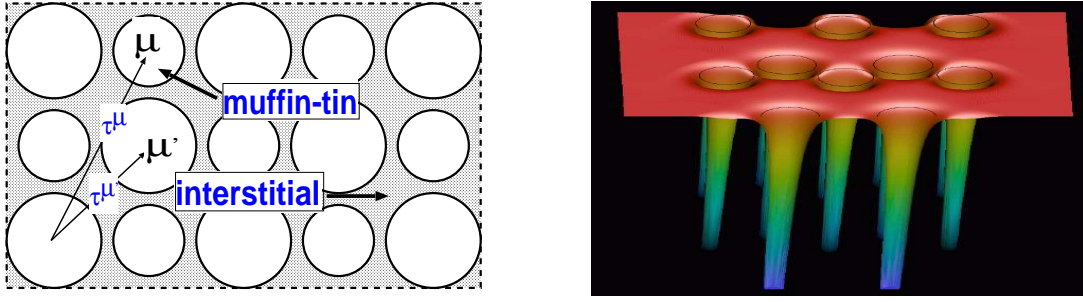


Fig. 10: Left figure: Volume of unit cell partitioned into muffin-tin spheres of two different types of atoms and the interstitial region. Right figure: Actual self-consistent effective potential as obtained from an FLAPW calculation.

puting power and parallelization strategies.

5.1 The APW Concept

There are many possible ways to solve the Kohn-Sham equations. Frequently, a variational method is chosen by which a wavefunction $\psi_{\mathbf{k},\nu}(\mathbf{r})$ of Bloch vector \mathbf{k} and band index ν is sought as a linear combination of basis functions $\varphi(\mathbf{r})$ satisfying the Bloch boundary conditions. The most straightforward choice would be to expand the wavefunction into planewaves or Fourier series, respectively,

$$\psi(\mathbf{k}, \nu) = \sum_{|\mathbf{k}+\mathbf{G}| \leq K_{\max}} c_{\mathbf{k},\nu}^{\mathbf{G}} \exp[i(\mathbf{k} + \mathbf{G})\mathbf{r}]. \quad (37)$$

Here \mathbf{G} are all reciprocal lattice vectors up to the largest value of K_{\max} and $c_{\mathbf{k},\nu}^{\mathbf{G}}$ are variational coefficients. The planewave basis set has some important advantages: Planewaves are orthogonal, they are diagonal in momentum space and the implementation of planewave based methods is rather straightforward due to their simplicity. The credit goes to Slater [30] having realized that owing to the singularity of the crystal potential at the nucleus, electron wavefunctions are varying very quickly near it, the planewave expansion would converge very slowly, large wavevectors (K_{\max}) would be needed to represent the wavefunctions accurately, which makes the set-up and diagonalization of the Hamiltonian matrix in terms of planewaves impracticable if not impossible. Even with the modern computer hardware, the planewaves are used only in the context of pseudopotential which allow an accurate description of the wavefunctions between the atoms, but avoid the fast oscillations near the core. Thus, less basis functions are needed.

In the APW method the space is partitioned into spheres centered at each atom site, the so-called muffin-tins (MTs), and into the remaining interstitial region (cf. Fig. 10). The MT spheres do not overlap and they are typically chosen such that they nearly (to allow for structural relaxations) fill the maximal possible space. Inside the muffin-tins, the potential is approximated to be spherically symmetric, and in many implementations the interstitial potential is set constant. The restrictions to the potential are commonly called shape-approximations. Noting that planewaves solve the Schrödinger equation in a constant potential, Slater suggested to replace the Bessel functions $j_l(Kr)$ in the Rayleigh decomposition of the planewave inside the sphere by radial functions $u_l(K, r)$, which match the Bessel functions in value at the sphere radius R_{MT} and whose product with the spherical harmonics $Y_L(\hat{\mathbf{r}})$ are the solutions in a spherical

potential. It is this procedure what is understood by the term augmentation. Thus, the single wavefunctions $\psi_{\mathbf{k},\nu}(\mathbf{r})$ are expressed as trial functions

$$\psi_{\mathbf{k},\nu}(\mathbf{r}) = \sum_{|\mathbf{G}+\mathbf{k}| \leq K_{\max}} c_{\mathbf{k},\nu}^{\mathbf{G}} \varphi_{\mathbf{G}}(\mathbf{k}, \mathbf{r}) \quad (38)$$

in terms of the APW basis functions:

$$\varphi_{\mathbf{G}}(\mathbf{k}, \mathbf{r}) = \begin{cases} e^{i(\mathbf{k}+\mathbf{G})\mathbf{r}} & \text{interstitial region} \\ \sum_{lm} a_L^{\mu\mathbf{G}}(\mathbf{k}) u_l(r^\mu|E) Y_L(\hat{\mathbf{r}}^\mu) & \text{muffin-tin } \mu \end{cases} \quad (39)$$

The position \mathbf{r} inside the spheres μ located at $\boldsymbol{\tau}^\mu$ (cf. Fig. 10) is given with respect to the center of each sphere. L abbreviates the quantum numbers l and m and u_l is the regular solution of the radial Schrödinger equation

$$\left\{ -\frac{\hbar^2}{2m} \frac{\partial^2}{\partial r^2} + \frac{\hbar^2}{2m} \frac{l(l+1)}{r^2} + V(r) - E \right\} r u_l(r) = 0 \quad (40)$$

to the energy parameter E_l . Here, $V(r)$ is the spherical component of the potential $V(\mathbf{r})$. The coefficients

$$a_L^{\mu\mathbf{G}}(\mathbf{k}) = a_L^\mu(\mathbf{k} + \mathbf{G}) = 4\pi \exp(i\mathbf{k}\boldsymbol{\tau}^\mu) i^l Y_L^*(\hat{\mathbf{K}}) \frac{j_l(KR^\mu)}{u_l(R^\mu)}, \quad \mathbf{K} = \mathbf{k} + \mathbf{G} \quad (41)$$

are determined from the requirement, that the wavefunctions are continuous at the boundary of the muffin-tin spheres in order for the kinetic energy to be well-defined. The variational coefficients $c^{\mathbf{G}}$ uniquely determine the wavefunction in the interstitial region.

If E were kept fixed, used only as a parameter during the construction of the basis, the Hamiltonian could be set up in terms of this basis. This would lead to a standard secular equation for the band energies where for a given \mathbf{k} -point in the Brillouin zone (BZ) a set of band energies E_ν are determined. Unfortunately, it turns out, that the APW basis does not offer enough variational freedom if E is kept fixed. An accurate description can only be achieved if the energies are set to the corresponding band energies $E_{\mathbf{k},\nu}$. In this case the Hamiltonian matrix H depends not only on \mathbf{k} , $H(\mathbf{k})$, but also on $E_{\mathbf{k},\nu}$, $H(E_{\mathbf{k},\nu})$, and the latter can no longer be determined by a simple diagonalization. Since the u_l 's depend then on the band energies, the solution of the secular equation becomes a nonlinear problem, which is computationally much more demanding than a secular problem. One way of solving this problem is to fix the energy E and scan over \mathbf{k} to find a solution, i.e. find one band at the time, instead of diagonalizing a matrix to find all the bands at a given \mathbf{k} . Thus, in Slater's formulation of the method E enters as an additional non-linear variational parameter varying the shape of the functions u_l till the optimal shape is found for the band energies $E_{\mathbf{k},\nu}$ one has looked for. There are several other limitations connected to the APW method. One is rather obvious, when $u_l(R)$ in Eq.(41) becomes zero at the MT boundary, the radial function and the planewave becomes decoupled, known as the asymptote problem. Others are beyond the scope of the chapter. Further information about the APW method can be found in the book by Loucks [32], which also reprints several early papers including Slater's original publication [30].

There is one remaining point. Please notice that the APW method produces per construction principle wavefunctions with a discontinuity in the slope at the muffin-tin boundary. Due to

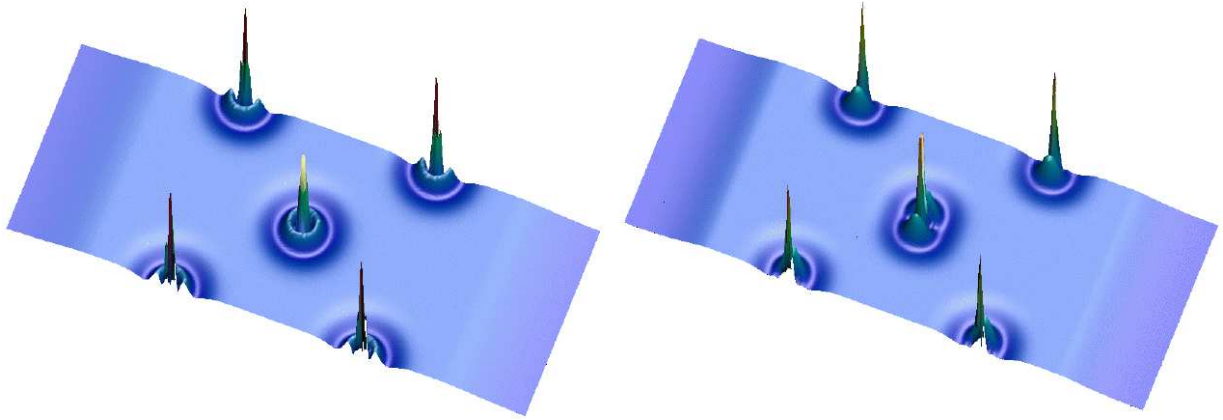


Fig. 11: Square of the LAPW basisfunction generated for $\mathbf{G} = 0$ and \mathbf{k} at the origin ($\bar{\Gamma}$ -point) (left) and boundary (\bar{M} -point) (right) of the Brillouin zone of a 3-layer thin film of Cu(100). The cuts are taken in the $\{110\}$ plane. The basisfunctions are optimally suited to represent 4s states of Cu (left) and 4p states (right).

these discontinuous first derivatives the secular equation in the APW basis

$$\sum_{\mathbf{G}'} (\langle \varphi_{\mathbf{G}} | \mathbf{H} - \varepsilon_{\mathbf{k}\nu} | \varphi_{\mathbf{G}'} \rangle + \langle \varphi_{\mathbf{G}} | \mathbf{T}_S | \varphi_{\mathbf{G}'} \rangle) c_{\mathbf{k}\nu}^{\mathbf{G}'} = 0 \quad (42)$$

contains a second term due to the matrix elements $\langle \psi | -\nabla^2 | \psi \rangle$ of the kinetic energy operator \mathbf{T} commonly defined as $\mathbf{T} = -\nabla^2$, which is replaced by $\langle \nabla \psi | \nabla \psi \rangle$, leading then via Green's theorem to the appearance of additional surface integrals $T_S \propto \int \psi^* \left[\left(\frac{\partial \psi}{\partial n} \right)_- - \left(\frac{\partial \psi}{\partial n} \right)_+ \right] dS$, where $+$ ($-$) indicates just outside and inside the muffin-tin sphere. The matrix elements of \mathbf{T}_S are proportional to the difference of the logarithmic derivatives from the function u_l , $D(u_l|E) = \frac{u_l'(R)}{u_l(R)}$, and that of an empty sphere $D(j_l|E) = \frac{j_l'(R)}{j_l(R)}$, taken at the sphere boundary. The logarithmic derivatives are related to the phase shifts in scattering events. Thus, the second term in Eq.(42) can be interpreted describing the scattering of a planewave coming from the crystal at the sphere of the atoms. It is well-known that the logarithmic derivatives and the phase shifts are energy dependent quantities, which explains the explicit energy dependence of the APW Hamiltonian in particular, and all nonlinear electronic structure methods in general.

5.2 The LAPW Basisfunctions

To avoid the problems connected with the APW method resulting from the energy dependence of the Hamiltonian, in the middle of the seventies linearized methods were invented by Andersen [20] and Koelling and Arbman [34]. Based on an idea proposed by Marcus [36], the basis functions u_l in the muffin-tins were supplemented by their energy derivatives \dot{u}_l , but both, u_l and \dot{u}_l , are now evaluated at a fixed energy E_l . The original energy dependence of the radial basis-function is thereby replaced by the Taylor series:

$$u_l(E) = u_l(E_l) + (E - E_l)\dot{u}_l(E_l) + \dots \quad (43)$$

terminated after the linear term. In this way, the wavefunctions are affected by an error which is quadratic in the deviation of the eigenvalue E from the energy parameter E_l , the error in the eigenvalues enter only to fourth order [34]. With this extension, the explicit form of the basis functions is now:

$$\psi_{\mathbf{G}}(\mathbf{k}) = \begin{cases} \exp(i(\mathbf{k} + \mathbf{G})\mathbf{r}) & \text{interstitial} \\ \sum_{l,m} (a_{lm}^{\mu,\mathbf{G}}(\mathbf{k})u_l^\mu(r) + b_{lm}^{\mu,\mathbf{G}}(\mathbf{k})\dot{u}_l^\mu(r))Y_{lm}(\hat{\mathbf{r}}^\mu) & \text{muffin-tin } \mu. \end{cases} \quad (44)$$

Examples of LAPW basisfunctions are shown in Fig. 11. The values of the coefficients $a_{lm}^{\mu,\mathbf{G}}(\mathbf{k})$ and $b_{lm}^{\mu,\mathbf{G}}(\mathbf{k})$ are determined to ensure continuity in value and derivative of the basis functions across the muffin-tin boundary. Thereby, also the surface integrals $\int \psi^* \left(\frac{\partial \psi}{\partial n} \right) dS$ which were encountered in the APW method disappear. In this way, the energy dependence of the Hamiltonian is removed, simplifying the eigenvalue problem, Eq.(15), to a standard problem of linear algebra. Instead of working with u_l and \dot{u}_l several LAPW implementations follow the ASW idea, working only with u_l but for two different energy parameters E_l and E_l' . As we see below working with u_l and \dot{u}_l is rather elegant.

If \hat{H}_{sp}^μ denotes the spherical Hamiltonian in Eq.(40), \dot{u} can be determined from the energy derivative of this equation at E_l :

$$\hat{H}_{sp}^\mu \dot{u}_l^\mu = E_l \dot{u}_l^\mu + u_l^\mu. \quad (45)$$

The normalization of the radial functions is usually chosen like: ¹

$$\int_0^{R^\mu} r^2 u_l^{\mu 2} dr = 1 \quad (46)$$

and the energy derivatives, \dot{u}_l^μ , are orthogonal to the radial functions, i.e.

$$\int_0^{R^\mu} r^2 u_l^\mu \dot{u}_l^\mu dr = 0 \quad (47)$$

a relation, which will simplify the calculation of the elements of the Hamilton matrix.

Stimulated by the idea of the LAPW basis set, one may ask to improve the basis set by matching only the 1st derivative continuously, but also higher derivatives working with higher energy derivatives of u_l . This approach has actually been followed by Takeda and Kübler [64] using n energy parameters to match the wavefunction continuously till the $(n - 1)$ st derivative. However, it turned out that such wavefunctions are variationally very stiff and the convergence of the results with respect of the number of basis functions is rather slow. This can be understood by following this procedure up to the extreme were the wavefunction matches to all derivatives. Then we know, the u_l must be the Bessel function j_l or the planewave, respectively. We have already argued before that this requires an infinite number of planewave to describe the wavefunction at the $1/r$ singularity. Thus, it is a great merit of the LAPW basis set, that the basis set is linear, but nearly as efficient as the APW method. The speed of convergence with respect to the number of basisfunctions can even be improved by the introduction of local orbitals.

¹In the many LAPW-codes, the electrons in the muffin-tin are treated in the scalar-relativistic approximation [49]. This means that a two-component wavefunction is used and the normalization conditions are modified accordingly. For the continuity conditions, only the “large component” of the radial function is taken into account. To keep the formalism as simple as possible, in the following we will discuss only the non-relativistic case.

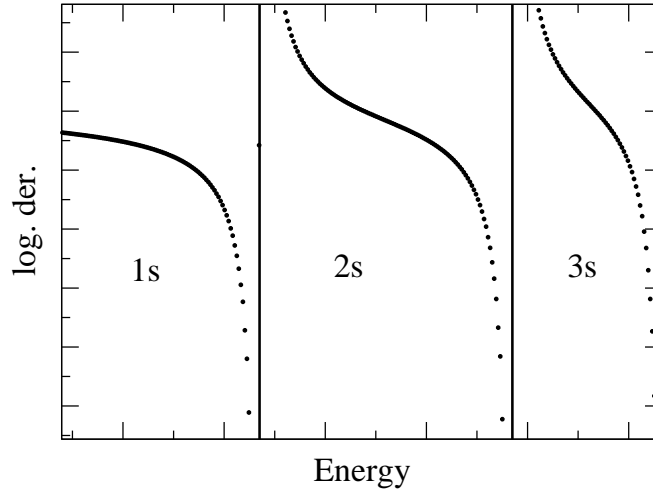


Fig. 12: Schematic drawing of the logarithmic derivative, $\frac{u_l'(R)}{u_l(R)}$, for $l = 0$ as function of the energy. The asymptotes indicate where the nodes of the wavefunction pass through the muffin-tin radius. They separate the branches labeled 1s, 2s and 3s.

The energies E_l are chosen to minimize the linearization errors, i.e. in the center of gravity of the l -like bands. It should be noticed here, that the choice of the energy parameter in a certain sense also determines the nodal structure of the wavefunction. A basis function, where the $l = 1$ energy parameter is chosen to describe a $2s$ -like wavefunction in a certain muffin-tin, will not be suitable to describe a $3s$ or a $1s$ state. The energy parameter is then said to be within the $2s$ branch (cf. Fig. 12). The flexibility of the basis function of course also depends on the size of the muffin-tin radius, R , so that with the choice of a smaller R in some cases two branches can be forced to “collapse” to a single branch [65]. On the other hand, a smaller flexibility allows to separate core- from valence states in a calculation. Thus, in a typical calculation only high-lying valence states are calculated (e.g. $3s$, $3p$, $3d$), while very localized states (e.g. $1s$, $2s$, $2p$) are excluded from the calculation. These states are then treated in a separate, atomic like, calculation using the $l = 0$ part of the muffin-tin potential.

As a final point, we will address the question how large l should be in a realistic calculation. Since the a and b coefficients in Eq.(44) should ensure continuity across the muffin-tin boundary, the plane-wave cutoff, G_{\max} and the l cutoff, l_{\max} , are normally chosen to match: A planewave with wavevector G_{\max} (given in inverse atomic units) has G_{\max}/π nodes per atomic unit. A spherical harmonic with $l = l_{\max}$ has $2l_{\max}$ nodes along a great circle on the muffin-tin sphere, i.e. there are $l_{\max}/(\pi R)$ nodes per atomic unit. Therefore, a reasonable choice of the cutoffs is $l_{\max} = RG_{\max}$, typically $l_{\max} = 8$ is chosen.

5.3 The FLAPW-Method in Film Geometry for Surfaces and Thin Films

Today, the physics of surfaces and films is an field of major interest and investigation. However, surfaces are difficult to treat, because they break the translational symmetry, i.e. there is only the 2-dimensional symmetry parallel to the surface left to be used to reduce the problem, and a semi-infinite problem is left perpendicular to the surface. In our approach surfaces are approximated by thin films, typically 10–15 atomic layers thick. Obviously, this approximation, which is called the thin-slab approximation, can only yield good results if the interaction between the two

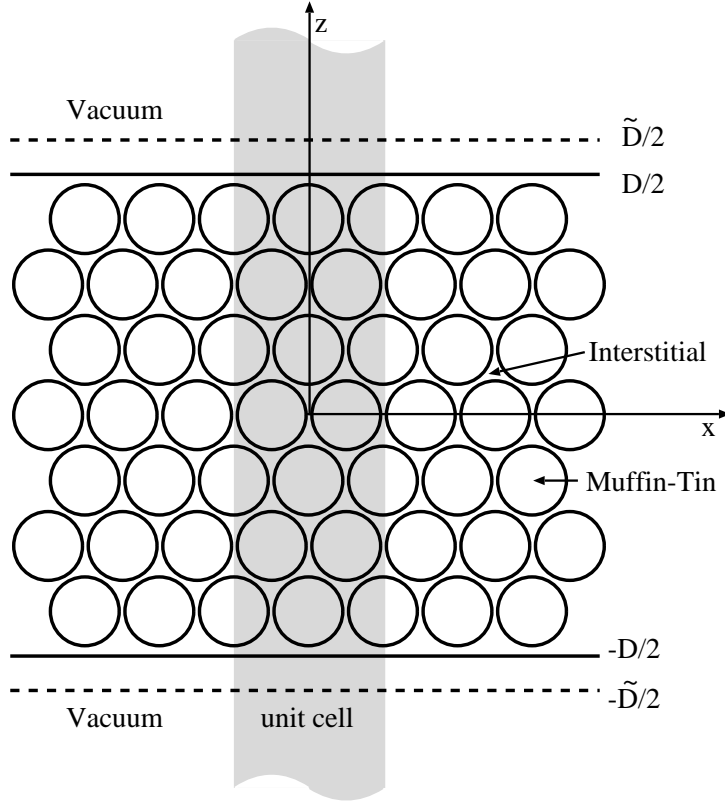


Fig. 13: The unit cell in film calculations contain two semi-infinite vacuum regions.

surfaces of the film is weak enough, so that each of them shows the properties of the surfaces of an ideal semi-infinite crystal. In the case of film calculations space is divided into three distinct regions, the muffin-tins, the interstitial and the vacuum region (cf. Fig. 13). The interstitial region now stretches from $-D/2$ to $D/2$ in z -direction, which is defined to be the direction perpendicular to the film. The representation of the wavefunctions inside the muffin-tin spheres remains exactly the same as in the bulk case. Since the periodicity along the z -direction is lost, the unit cell extends principally from $-\infty$ to ∞ in z -direction. Still the wavefunctions can be expanded in terms of planewaves. However, the wavevectors perpendicular to the film are not defined in terms of D , but in terms of \tilde{D} , which is chosen larger than D to gain greater variational freedom. Therefore, the planewaves have the form

$$\varphi_{\mathbf{G}_{\parallel} G_{\perp}}(\mathbf{k}_{\parallel}, \mathbf{r}) = e^{i(\mathbf{G}_{\parallel} + \mathbf{k}_{\parallel})\mathbf{r}_{\parallel}} e^{iG_{\perp}z} \quad \text{with} \quad G_{\perp} = \frac{2\pi n}{\tilde{D}}, \quad (48)$$

where \mathbf{G}_{\parallel} and \mathbf{k}_{\parallel} are the 2-dimensional wave- and Bloch vectors, \mathbf{r}_{\parallel} is the parallel component of \mathbf{r} and G_{\perp} is the wavevector perpendicular to the film. The basis functions in the vacuum region are constructed in the same spirit as the functions in the muffin-tins. They consist of planewaves parallel to the film, and a z -dependent function $u_{\mathbf{G}_{\parallel}}(\mathbf{k}_{\parallel}, z)$, which solves the corresponding one-dimensional Schrödinger equation Eq.(49), plus its energy derivative $\dot{u}_{\mathbf{G}_{\parallel}}(\mathbf{k}_{\parallel}, z)$.

$$\left\{ -\frac{\hbar^2}{2m} \frac{\partial^2}{\partial z^2} + V_0(z) - E_{vac} + \frac{\hbar^2}{2m} (\mathbf{G}_{\parallel} + \mathbf{k}_{\parallel})^2 \right\} u_{\mathbf{G}_{\parallel}}(\mathbf{k}_{\parallel}, z) = 0 \quad (49)$$

E_{vac} is the vacuum energy parameter and $V_0(z)$ is the planar averaged part of the vacuum potential. As in the case of \dot{u}_l in the muffin-tins, the function $\dot{u}_{\mathbf{G}_{\parallel}}(\mathbf{k}_{\parallel}, z)$ is calculated from a Schrödinger-like equation, which can be obtained by deriving Eq.(49) with respect to the energy.

$$\left\{ -\frac{\hbar^2}{2m} \frac{\partial^2}{\partial z^2} + V_0(z) - E_{vac} + \frac{\hbar^2}{2m} (\mathbf{G}_{\parallel} + \mathbf{k}_{\parallel})^2 \right\} \dot{u}_{\mathbf{G}_{\parallel}}(\mathbf{k}_{\parallel}, z) = u_{\mathbf{G}_{\parallel}}(\mathbf{k}_{\parallel}, z) \quad (50)$$

The resulting basis functions have the form

$$\varphi_{\mathbf{G}_{\parallel}G_{\perp}}(\mathbf{k}_{\parallel}, \mathbf{r}) = \left\{ a_{\mathbf{G}_{\parallel}G_{\perp}}(\mathbf{k}_{\parallel}) u_{\mathbf{G}_{\parallel}}(\mathbf{k}_{\parallel}, z) + b_{\mathbf{G}_{\parallel}G_{\perp}}(\mathbf{k}_{\parallel}) \dot{u}_{\mathbf{G}_{\parallel}}(\mathbf{k}_{\parallel}, z) \right\} e^{i(\mathbf{G}_{\parallel} + \mathbf{k}_{\parallel})\mathbf{r}_{\parallel}} \quad (51)$$

The coefficients $a_{\mathbf{G}_{\parallel}G_{\perp}}(\mathbf{k}_{\parallel})$ and $b_{\mathbf{G}_{\parallel}G_{\perp}}(\mathbf{k}_{\parallel})$ are determined in exactly the same way as it is done for the muffin-tins by requiring that the functions are continuous and differentiable at the vacuum boundary. It should be mentioned, that the vacuum basis functions offer less variational freedom than the basis set in the interstitial region does. This can be seen by noting that there are only two functions, $u_{\mathbf{G}_{\parallel}}$ and $\dot{u}_{\mathbf{G}_{\parallel}}$ times the corresponding planar planewave, to be matched to all planewaves of the interstitial region with the same \mathbf{G}_{\parallel} . But there are generally far more than two different G_{\perp} 's, i.e the number of basis functions in the vacuum region is significantly smaller than in the interstitial region. However, this can be improved rather easily. In Eq.(49) only one energy parameter E_{vac} is used. Instead one can use a whole series of parameters E_{vac}^i to cover an energy region. A possible choice of the energy parameters could be $E_{vac}^i = E_{vac}^{G_{\perp}} = E_{vac} - \frac{\hbar^2}{2m} G_{\perp}^2$, which leads correspondingly to G_{\perp} dependent basis functions $u_{\mathbf{G}_{\parallel}G_{\perp}}(\mathbf{k}_{\parallel}, z)$. For more details see Ref. [67]. In general, however, the present approximations is accurate, the energy spectrum of the electrons in the vacuum region is small due to the work-function.

Finally we would like to summarize the basis set used for thin film calculation with the FLAPW method.

$$\varphi_{\mathbf{G}_{\parallel}G_{\perp}}(\mathbf{k}_{\parallel}, \mathbf{r}) = \begin{cases} e^{i(\mathbf{G}_{\parallel} + \mathbf{k}_{\parallel})\mathbf{r}_{\parallel}} e^{iG_{\perp}z} & \text{interstitial} \\ \left\{ a_{\mathbf{G}_{\parallel}G_{\perp}}(\mathbf{k}_{\parallel}) u_{\mathbf{G}_{\parallel}}(\mathbf{k}_{\parallel}, z) + b_{\mathbf{G}_{\parallel}G_{\perp}}(\mathbf{k}_{\parallel}) \dot{u}_{\mathbf{G}_{\parallel}}(\mathbf{k}_{\parallel}, z) \right\} e^{i(\mathbf{G}_{\parallel} + \mathbf{k}_{\parallel})\mathbf{r}_{\parallel}} & \text{vacuum} \\ \sum_L a_L^{\mu\mathbf{G}}(\mathbf{k}) u_l(r) Y_L(\hat{\mathbf{r}}) + b_L^{\mu\mathbf{G}}(\mathbf{k}) \dot{u}_l(r) Y_L(\hat{\mathbf{r}}) & \text{MT}^{\mu} \end{cases} \quad (52)$$

This expansion has been suggested by H. Krakauer, M. Posternak and A. J. Freeman [45].

The expansion of the charge density n and the potential is very similar to expansion of the wavefunction. In the interstitial-region the two quantities are expanded into three-dimensional planewaves, inside the muffin-tins they are represented by spherical harmonics and radial functions, which are stored on an exponential mesh and in the vacuum they are expanded into two-dimensional planewave and z-depended functions. Of course, the charge density and the potential posses the lattice symmetry. Therefore, the expansion into planewaves is more general than necessary. The planewaves can be replaced by symmetrized planewaves, the so called stars Φ_s^{3D} for the interstitial region and the two-dimensional stars $\Phi_s^{2D}(\mathbf{r})$ for the vacuum region. Thus, the charge density and potential is expanded in the form:

$$n(\mathbf{r}) = \begin{cases} \sum_s n_s \Phi_s^{3D}(\mathbf{r}) & \mathbf{r} \in \text{interstitial region} \\ \sum_s n_s(z) \Phi_s^{2D}(\mathbf{r}) & \mathbf{r} \in \text{vacuum} \\ \sum_{\nu} n_{\nu}^{\mu}(r) K_{\nu}(\hat{\mathbf{r}}) & \mathbf{r} \in \text{MT}^{\mu} \end{cases} \quad (53)$$

and the Hamiltonian and overlap matrix consists now of three terms: the interstitial, muffin-tin sphere and the vacuum contribution, paying tribute that the space is now partitioned in three regions

$$H = H_I + H_{MT} + H_V \quad \text{and} \quad S = S_I + S_{MT} + S_V. \quad (54)$$

$n_s(z)\Phi_s^{2D}$ contain important information for the analysis and interpretation of STM topography and spectroscopy results on the basis of the Tersoff-Hamann model [68] as worked out by Heinze *et al.* [69].

6 The Green function method of Korringa, Kohn and Rostoker

The multiple-scattering method of Korringa, Kohn and Rostoker (KKR) for the calculation of the electronic structure of materials was introduced in 1947 by Korringa [73] and in 1954 by Kohn and Rostoker [74]. In order to solve the Schrödinger equation, the scattering properties of each scattering center (atom) are determined in a first step and described by a scattering matrix, while the multiple-scattering by all atoms in the lattice is determined in a second step by demanding that the incident wave at each center is the sum of the outgoing waves from all other centers. In this way, a separation between the potential and geometric properties is achieved.

A further significant development of the KKR scheme came when it was reformulated as a KKR Green function method [75, 76]. By separating the single-site scattering problem from the multiple-scattering effects, the method is able to produce the crystal Green function efficiently by relating it to the Green function of free space via the Dyson equation. In a second step the crystal Green function can be used as a reference in order to calculate the Green function of an impurity in the crystal [77], again via a Dyson equation. This way of solving the impurity problem is extremely efficient, avoiding the construction of huge supercells which are needed in wavefunction methods.

The development of *screened*, or *tight-binding*, KKR was a further breakthrough for the numerical efficiency of the method [78]. Via a transformation of the reference system remote lattice sites are decoupled, and the principal layer technique allows the calculation time to scale linearly with the number of atoms. This is especially useful for layered systems (surfaces, interfaces, multilayers) and allows the study of, e.g., interlayer exchange coupling or ballistic transport through junctions.

A short list of successful applications of the KKR method for electronic structure of solids, combined with density-functional theory, includes bulk materials [80], surfaces [81], interfaces and tunnel junctions [82], and impurities in bulk and on surfaces [83]. Spectroscopic properties [84] and transport properties [79, 85] have also been studied within this method. The KKR scheme can incorporate the Dirac equation, whenever relativistic effects become important [86] and was also applied to treat non-collinear magnetism [87].

6.1 Green Function Method

In density functional calculations the solution of the Kohn-Sham equations for the single particle wave functions $\varphi_\alpha(\mathbf{r})$ and the corresponding eigenvalues ε_α , the single particle energies, represents the central problem. Thus most of electronic structure calculations follow this route,

i.e. calculating eigenfunctions φ_α and eigenvalues ε_α . However, the calculation of φ_α and ε_α can be avoided, if instead the single particle Green function $G(\mathbf{r}, \mathbf{r}'; E)$ of the Kohn-Sham equation is determined, since this quantity contains all the information about the ground state. In particular the charge density and the local density of states can be directly calculated from the Green function, which is the solution of the Schrödinger equation for an energy E with a source at position \mathbf{r}' :

$$(-\partial_r^2 + V(\mathbf{r}) - E) G(\mathbf{r}, \mathbf{r}'; E) = -\delta(\mathbf{r} - \mathbf{r}') \quad , \quad (55)$$

with atomic units $\hbar^2/2m = 1$ used. Using the spectral representation for the (retarded) Green function

$$G(\mathbf{r}, \mathbf{r}'; E + i\epsilon) = \sum_{\alpha} \frac{\psi_{\alpha}(\mathbf{r})\psi_{\alpha}^*(\mathbf{r}')}{E + i\epsilon - E_{\alpha}} \quad (56)$$

it is easy to show that the charge density $n(\mathbf{r})$ can be directly expressed by an energy integral over the imaginary part of the Green function:

$$n(\mathbf{r}) = 2 \sum_{\substack{\alpha \\ E_{\alpha} < E_F}} |\psi_{\alpha}(\mathbf{r})|^2 = -\frac{2}{\pi} \int^{E_F} dE \operatorname{Im} G(\mathbf{r}, \mathbf{r}; E) \quad (57)$$

This relation directly allows calculation of the charge density from the imaginary part of the Green function, which can be interpreted as the local density of states at the position \mathbf{r} . The local density of states of a particular atom in a volume V is obtained by integrating over this volume

$$n_V(E) = -\frac{2}{\pi} \int_V d\mathbf{r} \operatorname{Im} G(\mathbf{r}, \mathbf{r}; E) \quad (58)$$

In this way the evaluation of the wave-functions $\psi_{\alpha}(\mathbf{r})$ can be avoided. Due to the strong energy-dependent structure of the density of states, the evaluation of the energy integral is usually very cumbersome and typically about 10^3 energy points are needed in an accurate evaluation of this integral.

The numerical effort can be strongly decreased, if the analytical properties of the Green function $G(z)$ for complex energies $z = E + i\Gamma$ are used. Since $G(z)$ is analytical in the whole complex energy plane, the energy integral can be transformed into a contour integral in the complex energy plane

$$n(\mathbf{r}) = -\frac{2}{\pi} \operatorname{Im} \int_{E_B}^{E_F} dz G(\mathbf{r}, \mathbf{r}; z) \quad (59)$$

where the contour starts at an energy E_B below the bottom of the valence bands, goes into the complex plane and comes back to the real axis at the Fermi level. Since for complex energies all structures of the Green function are broadened by the imaginary part Γ , the contour integral can be accurately evaluated using rather few energy points, typically 20-30, leading to a large saving of computer time. In this way Green function methods are competitive to diagonalization methods. Additional advantages occur for systems with two- or three-dimensional symmetry, since as a result of the energy broadening the \mathbf{k} -integration over the Brillouin zone requires for complex energies much less \mathbf{k} -points. In the evaluation of the contour integral, special care is necessary for the piece of the path close to E_F , since here the full structure of $G(E)$ on the real axis reappears. Therefore the energy mesh should become increasingly denser when approaching E_F .

The integration over a complex energy contour can also be extended to finite temperatures by using the analytical properties of the Fermi-Dirac distribution. Here the essential point is that the contour close to E_F is replaced by a sum over Matsubara energies $z_j = E_F + i\pi(2j-1)kT$, $j = 1, 2, \dots$. Then only complex energies are needed, since the energy point closest to E_F has still an imaginary part of πkT . This is of particular advantage, when a discrete k -mesh is used, like e.g. in the special points method.

The real problem is the evaluation of the Green function for the system of interest. Since we want to avoid evaluation of all eigenvalues ε_α and wave functions φ_α we rather calculate the Green function G

$$G(E) = \frac{1}{E + i\varepsilon - H} = \frac{1}{E + i\varepsilon - H_o - V} \quad (60)$$

of a system with Hamiltonian $H = H_o + V$ to the Green function $G_o = \{E + i\varepsilon - H_o\}^{-1}$ of a reference system, which is analytically known or easy to calculate. Then $G(E)$ can be obtained from the Dyson equation

$$G(E) = G_o(E) + G_o(E) V G(E) = G_o \frac{1}{1 - VG_o} \quad (61)$$

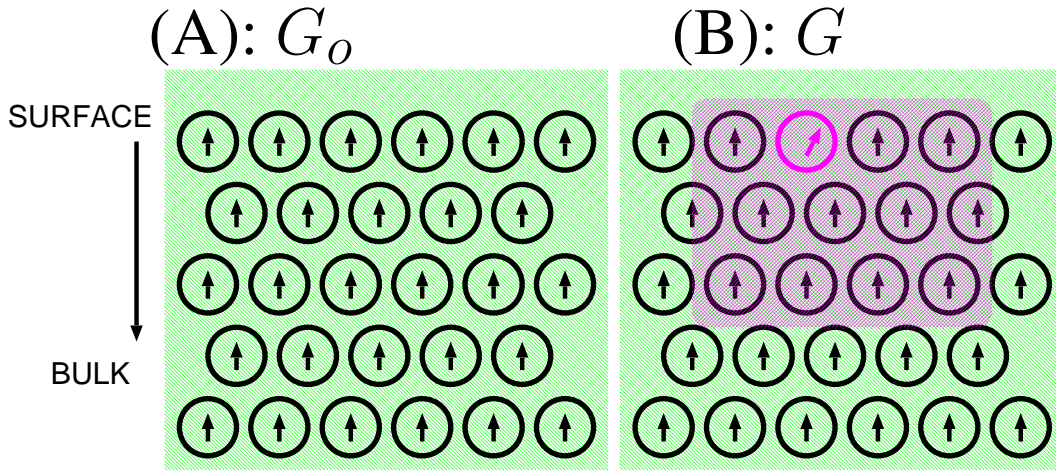


Fig. 14: (A) is a schematic view of a host system prototype showing a perfect surface characterized by collinear magnetism while (B) is a schematic view of a system characterized by two perturbations: first by the presence of an impurity sitting in the surface layer and second by taking into account noncollinear magnetism. The extension of the perturbation is delimited by a pink color.

For instance, for a bulk crystal one starts with the free space Green function $G_o(H_o = -\partial_{\mathbf{r}}^2)$, such that V is the sum of the potentials of all atoms. For the surface Green function, G_o is identified with the bulk Green function, such that V is the difference between the potentials at the surface and in the bulk. Analogously for a cluster of adatoms on a surface one starts again with the surface Green function G_o (Fig.14), such that V represents the change of the ad-cluster potential with respect to the surface potential including the perturbation of the potentials of the neighboring host atoms. Most important is, that the perturbed potential V is well localized near the impurities, while the perturbed wavefunctions are not localized and accurately described by the Dyson equation.

Such impurity problems are often described by an 'Ersatzgeometry', e.g. an impurity in a relatively small cluster of atoms or by a supercell geometry with a periodic array of impurities. In these cases the boundary conditions for the wave functions are changed violently, since e.g. for a cluster all wave functions are restricted to the size of the cluster. Therefore the introduction of the host Green function G_o solves the so-called "embedding problem", since it correctly describes the embedding of the impurity in the infinite surface system.

6.2 KKR representation of the Green function

As mentioned earlier, in the method of Korringa, Kohn and Rostoker (KKR) [75] the Schrödinger equation is solved by multiple scattering theory, describing the propagation of a wave in the solid as a repetition of single scattering events at the different atoms. Thus first the single scattering event of the wave at the potential of the different single atoms n is calculated, described by the single site "t-matrix" t_n , and then the multiple scattering at the given arrangement of the atoms in the crystal. The resulting equations show a beautiful separation between potential and structural properties, which are typical for the KKR method. In the following we summarize the most important results.

In the KKR-Green function method one divides the whole space into non-overlapping and space-filling cells centered at positions \mathbf{R}^n (similar to Fig. 10). In each cell the electrons are scattered by potentials v^n , which in this section are assumed to be spherically symmetric and centered at \mathbf{R}^n . By introducing cell-centered coordinates the Green function $G(\mathbf{r} + \mathbf{R}^n, \mathbf{r}' + \mathbf{R}^{n'}; E)$ can then be expanded in each cell as a function of \mathbf{r} and \mathbf{r}' into spherical harmonics:

$$\begin{aligned} G(\mathbf{R}_n + \mathbf{r}, \mathbf{R}_{n'} + \mathbf{r}'; E) = & -i\sqrt{E} \sum_L R_L^n(\mathbf{r}_<; E) H_L^n(\mathbf{r}_>; E) \delta_{nn'} \\ & + \sum_{LL'} R_L^n(\mathbf{r}; E) G_{LL'}^{nn'}(E) R_{L'}^{n'}(\mathbf{r}'; E) \end{aligned} \quad (62)$$

Here \mathbf{r} and \mathbf{r}' are restricted to the cells n and n' and $\mathbf{r}_<$ and $\mathbf{r}_>$ denote the one of the two vectors \mathbf{r} and \mathbf{r}' which has the smaller or larger absolute value. The $R_L^n(\mathbf{r}; E)$ and $H_L^n(\mathbf{r}; E)$ are the product of spherical harmonics and radial eigenfunctions to the central potential $v^n(r)$:

$$R_L^n(\mathbf{r}; E) = R_L^n(r; E) Y_L(\hat{r}), \quad (63)$$

$$H_L^n(\mathbf{r}; E) = H_L^n(r; E) Y_L(\hat{r}). \quad (64)$$

Here $R_L^n(\mathbf{r}, E)$ is the regular solution which varies at the origin as r^l and which represents the solution for an incoming spherical Bessel function $j_l(\sqrt{E}r)Y_L(\hat{r})$, while H_L^n is the corresponding irregular solution varying as $1/r^{l+1}$ at the origin and being identical with the spherical Hankel function $h_l(\sqrt{E}r)$ outside the range of the potential. Both radial functions are connected by the Wronskian relation, which guarantees that the first term in Eq.(62) represents the exact Green function for the single potential $v^n(r)$ in free space. Since this term satisfies already the source condition $-\delta(\mathbf{r} - \mathbf{r}')$ for the Green function of Eq.(55), the second term is source free and contains in the double angular momentum expansion only the regular solutions R_L^n and $R_{L'}^{n'}$. By construction, the expression (62) for the Green function satisfies in each cell n the general solution of the Schrödinger equation (55) for the Green function, while the matrix $G_{LL'}^{nn'}(E)$, the so-called *structural Green function*, describes the connection of the solutions in the different cells and thus contains all the information about the multiple scattering problem, which is in this

way reduced to the solution of an algebraic problem. The clear separation between the single-site properties, described by the radial solutions $R_L^n(\mathbf{r})$ and $H_L^n(\mathbf{r})$ and the multiple scattering properties as described by the matrix $G_{LL'}^{nn'}$, is the main advantage of the KKR method.

In principle, the structural Green function matrix $G_{LL'}^{nn'}(E)$ can be determined by matching the solutions of the neighboring cells at the cell boundaries. However at the cell boundaries the angular momentum expansion converges rather slowly, so that presumably a large l_{\max} cut-off would be needed. The more elegant and at the same time more efficient way consists in using the power of multiple scattering theory, where the Green function is basically only needed in the inner region of the cell, where the potential is strong, so that the l -convergence represents no problem. As shown by Beeby and others [75], the structural Green function matrix can be determined from the corresponding matrix g in free space by the Dyson equation

$$G_{LL'}^{nn'}(E) = g_{LL'}^{nn'}(E) + \sum_{n''L''} g_{LL''}^{nn''}(E) t_{l''}^{n''}(E) G_{L''L'}^{n''n'}(E) \quad (65)$$

where the t -matrix t_l^n for the potential $v^n(r)$ is given by

$$t_l^n(E) = \int_0^R r^2 dr j_l(\sqrt{E}r) v^n(r) R_l^n(r; E) \quad (66)$$

The derivation of this equation is lengthy and straightforward, so that we refer for this to the literature cited above. An elementary derivation, valid also for the full-potential case, has been given by Zeller [88].

In practice, the host structural Green functions are first calculated in \mathbf{k} -space using matrix inversion; a subsequent Fourier transform gives us the real-space quantities. We write, then,

$$\overset{\circ}{G}_{LL'}(\mathbf{k}; E) = \sum_{n'} \overset{\circ}{G}_{LL'}^{nn'}(E) e^{-i\mathbf{k} \cdot (\mathbf{R}^n - \mathbf{R}^{n'})} \quad (67)$$

(which, due to translational symmetry, is independent of n). The algebraic Dyson equation Eq.(65) becomes

$$\overset{\circ}{G}_{LL'}(\mathbf{k}; E) = g_{LL'}(\mathbf{k}; E) + \sum_{L''} g_{LL''}(\mathbf{k}; E) t_{l''}(E) \overset{\circ}{G}_{L''L'}(\mathbf{k}; E) \quad (68)$$

(the t -matrix is independent of n , again due to translational symmetry). Here $g_{LL'}$ are the reference structural green function of the original system before perturbing it by the surface. This original system can be for example free space. The structural Green functions $G_{LL'}$ and $g_{LL'}$, and the t -matrix t_l , are considered as matrices in L and L' , and (68) is solved by matrix inversion after a cutoff at some $l = l_{\max}$ for which the t -matrix becomes negligible (usually $l_{\max} = 3$ or 4 suffices). The result is

$$\overset{\circ}{G}_{LL'}^{nn'}(E) = \frac{1}{V_{\text{BZ}}} \int_{\text{BZ}} d^3k e^{i\mathbf{k} \cdot (\mathbf{R}^n - \mathbf{R}^{n'})} \left[\left(1 - \mathbf{g}(\mathbf{k}; E) \mathbf{t}(E) \right)^{-1} \mathbf{g}(\mathbf{k}; E) \right]_{LL'} \quad (69)$$

where the integral is over the Brillouin zone volume V_{BZ} . For the calculation of the charge density or of the density of states, only the on-site term $n = n'$, $G_{LL}^{nn}(E)$, is needed.

Here, the t -matrix $\mathbf{t}(E)$ depends on the atom-type μ and on angular-momentum indexes (it is site-diagonal, $(\mathbf{t})_{l'}^{\mu\mu'} = t_l^n \delta_{\mu\mu'}$). The structure constants $\mathbf{g}(\mathbf{k}; E)$ are considered as a matrices in both (L, L') and (μ, μ') , and thus the computational effort for the matrix inversion increases as $O(N_{\text{at}}^3)$. A considerable speed-up can be achieved for large systems by using the concept of the screening transformation.

6.3 Two-dimensional systems: finite-thickness slabs and half-infinite crystals

The extension of the KKR method to the treatment of layered systems, such as surfaces and interfaces, is straightforward, and most efficient within the screened KKR formalism, where $O(N)$ scaling can be achieved (where N is the number of layers).

When treating a layered system, a surface-adapted geometry is used, in the sense that the two-dimensional periodicity of the atomic layers parallel to the surface (or interface) is exploited while the direction perpendicular to these layers is treated as if these were different atoms in a unit cell. The Fourier transforms are done now within the two-dimensional surface Brillouin zone (SBZ), and the corresponding integration is over all \mathbf{k}_{\parallel} in the SBZ. Thus, we have

$$\begin{aligned} \overset{\circ}{G}_{LL'}^{n\mu, n'\mu'}(E) &= \frac{1}{A_{\text{SBZ}}} \int_{\text{SBZ}} d^2 k_{\parallel} e^{i\mathbf{k}_{\parallel} \cdot (\mathbf{R}^n - \mathbf{R}^{n'})} e^{i\mathbf{k}_{\parallel} \cdot (\bar{\chi}^{\mu} - \bar{\chi}^{\mu'})} \\ &\times \left[(1 - \mathbf{G}^r(\mathbf{k}_{\parallel}; E) \Delta \mathbf{t}(E))^{-1} \mathbf{G}^r(\mathbf{k}_{\parallel}; E) \right]_{LL'}^{\mu\mu'}. \end{aligned} \quad (70)$$

where now \mathbf{R}^n are in-plane position vectors of the two-dimensional Bravais lattice, while $\bar{\chi}^{\mu}$ are vectors connecting atomic positions in different layers; A_{SBZ} is the area of the SBZ.

In the case of surfaces, the vacuum is described by empty sites, meaning that the lattice structure is continued into the vacuum but no nuclei are positioned there. In this way, the vacuum potential and charge density are calculated within the multiple-scattering formalism on the same footing as the bulk. In practice, three or four monolayers of vacuum sites are enough for the calculation of the electronic structure; Eq.(70) can be cut-off after that.

Depending on the problem, one can choose to use a slab of finite thickness in order to represent a surface or interface, or one can choose to take half-infinite boundary conditions. In the latter case, and starting from a “boundary” layer, the crystal is continued by periodically repeating the potential of this boundary layer to all subsequent layers up to infinity. One is then faced with a problem of inverting an infinite matrix, which due to the screening transformation has a tridiagonal form, in order to find the Green function in the region of interest. This is done efficiently by the decimation technique [89], which is based on an iterative inversion of matrices of doubled size at each step. In this way the number of layers which are included in the Green function grows exponentially with the number of steps, and the limit of the half-infinite crystal is rapidly achieved.

Once the structural Green function $\overset{\circ}{G}_{LL'}^{nn'}(E)$ of the ideal crystal is known (e.g. surface), the Green function $G_{LL'}^{nn'}(E)$ for the crystal with impurity can be evaluated by a modified Dyson equation

$$G_{LL'}^{nn'} = \overset{\circ}{G}_{LL'}^{nn'} + \sum_{n''L''} \overset{\circ}{G}_{LL''}^{nn''} \Delta t_{L''}^{n''} G_{L''L'}^{n''n'} \quad , \quad \Delta t_L^n = t_L^n - \overset{\circ}{t}_L^n \quad (71)$$

where Δt_L^n is the difference $t_L^n - \overset{\circ}{t}_L^n$ between the t -matrices in the perturbed and in the ideal lattice. Since this difference, determined by the perturbation of the potential, is restricted to the vicinity of the impurity, the Green function in this subspace can be easily determined in real space by matrix inversion. The rank of the matrices to be inverted is given by the number n_d of perturbed potentials times the number $(l_{\text{max}} + 1)^2$ of angular momenta used. Here l_{max} is the maximum angular momentum used in the calculations, e.g. $l_{\text{max}} = 3$.

For a single impurity it is often sufficient to neglect the perturbation of the neighboring host atoms and to take into account in Eq.(71) only the perturbation due to the impurity potential

into account. This so-called single site approximation gives a quite reasonable description of the electronic structure of the impurity and is the essential ingredient of the coherent potential approximation for random alloys. For a more accurate description the perturbations of the neighbors have to be included. The size of the perturbation naturally increases, if impurity pairs, trimers or larger clusters of impurities are included. One should finally add that the structural Green function $\overset{\circ}{G}_{LL'}^{nn'}$ describes the correct embedding in the local environment. Therefore the calculation of $\overset{\circ}{G}_{LL'}^{nn'}$ represents the high entrance fee one has to pay in Green function calculations.

Acknowledgments

I thank Samir Lounis for his help in preparing this manuscript.

References

- [1] K. Reuter, C. Stampfl, and M. Scheffler, *Methods*, in *Handbook of Materials Modeling*, Part A, S. Yip Ed. (Springer, Berlin, 2005).
- [2] H. Hohenberg and W. Kohn, Phys. Rev. **136**, B864 (1964).
- [3] R. M. Dreizler and J. da Providencia, (Plenum, New York, 1985).
- [4] R. O. Jones and O. Gunnarsson, Rev. Mod. Phys. **61**, 689 (1989).
- [5] M. Ernzerhof, J. P. Perdew and K. Burke, *Density Functionals: Where do they come from, why do they work?*, in *Topics in Current Chemistry*, Vol. 180, R.F. Nalewajski Ed. (Springer, Berlin, 1996).
- [6] M. Wuttig, Y. Gauthier, S. Blügel, Phys. Rev. Lett. **70**, 3619 (1993).
- [7] W. Kohn and L.J. Sham, Phys. Rev. **140**, A1133 (1965).
- [8] S. Blügel, (PhD thesis, RWTH Aachen, 1988).
- [9] L. Hedin and B. I. Lundqvist, J. Phys. C (Solid State Physics) **4**, 2064 (1971).
- [10] S. H. Vosko and L. Wilk and N. Nusair, Can. J. Phys. **58**, 1200 (1980).
- [11] J. P. Perdew, J. A. Chevary, S. H. Vosko, K. A. Jackson, M. R. Pederson, D. J. Singh, and C. Fiolhais, Phys. Rev. B **46**, 6671 (1992).
- [12] J. P. Perdew, K. Burke, and M. Ernzerhof, Phys. Rev. Lett. **77**, 3865 (1996).
- [13] J. Stoer, *Numerische Mathematik I*, (Springer-Verlag, Berlin, 1994).
- [14] D. J. Chadi and Marvin L. Cohen, Phys. Rev. B **8**, 5747 (1973).
- [15] S. L. Cunningham, Phys. Rev. B **10**, 4988 (1974).
- [16] O. Jepsen and O. K. Andersen, Solid State Commun. **9**, 1763 (1971).
- [17] G. Lehmann and M. Taut, phys. stat. sol. (b) **54**, 469 (1972).
- [18] P. E. Blöchl, O. Jepsen, and O. K. Andersen, Phys. Rev. B **49**, 16223 (1994).
- [19] R. Pentcheva, *Ab-initio Rechnungen zum Zusammenhang zwischen Magnetismus und Struktur ultradünner Filme*, (Diploma thesis, RWTH Aachen, 1995).
- [20] O. K. Andersen, Phys. Rev. B **12**, 3060 (1975).
- [21] A. R. Williams, J. Kübler, and C. D. Gelatt Jr., Phys. Rev. B **19**, 6094 (1979).
- [22] H. Akai, M. Akai, S. Blügel, B. Drittler, H. Ebert, K. Terakura, R. Zeller, and P. H. Dederichs, Prog. Theo. Phys. (Suppl) **101**, 11 (1990).
- [23] E. Wimmer and A. J. Freeman, *Fundamentals of Electronic Structure of Surfaces*, in *Handbook of Surface Science*, Vol. 2, K. Horn and M. Scheffler Eds. (Springer, Berlin, 2000).

- [24] D. Wortmann, H. Ishida, and S. Blügel, Phys. Rev. B **65**, 165103 (2002).
- [25] D. Wortmann, H. Ishida, and S. Blügel, Phys. Rev. B **65**, 165103 (2002).
- [26] E. E. Krasovskii, Phys. Rev. B **70**, 245322 (2004).
- [27] E. Wimmer, H. Krakauer, M. Weinert, and A. J. Freeman, Phys. Rev. B **24**, 864 (1981).
- [28] M. Weinert, E. Wimmer, and A. J. Freeman, Phys. Rev. B **26**, 4571 (1982).
- [29] D. Singh, *Planewaves, Pseudopotentials and the LAPW Method*, (Kluwer Academic Publishers, Boston/Dordrecht/London, 1994).
- [30] J. C. Slater, Phys. Rev. **51**, 846 (1937).
- [31] J. C. Slater, *Advances in Quantum Chemistry* **1**, 35 (1964).
- [32] T. Loucks, *Augmented Plane Wave Method*, (Benjamin, New York, 1967).
- [33] H. Bross, G. Bohn, G. Meister, W. Schubo, and H. Stohr, Phys. Rev. B **2**, 3098 (1970).
- [34] D. D. Koelling and G. O. Arbman, J. Phys. F (Metal Phys.) **5**, 2041 (1975).
- [35] R. V. Kasowski, Phys. Rev. B **8**, 1378 (1973).
- [36] P. M. Marcus, Int. J. Quantum Chem. Suppl. **1**, 567 (1967).
- [37] M. Weinert, *Solution of Poisson's equation: beyond Ewald-type methods*, J. Math. Phys. **22**, 2433 (1981).
- [38] D. R. Hamann, Phys. Rev. Lett. **42**, 662 (1979).
- [39] H. J. F. Jansen and A. J. Freeman, Phys. Rev. B **30**, 561 (1984).
- [40] S.-H. Wei, H. Krakauer, and M. Weinert, Phys. Rev. B **32**, 7792 (1985).
- [41] S.-H. Wei and H. Krakauer, Phys. Rev. Lett. **55**, 1200 (1985).
- [42] L. F. Mattheiss and D. R. Hamann, Phys. Rev. B **33**, 823 (1986).
- [43] P. Blaha, K. Schwarz, P. Sorantin and S.B. Trickey, Comp. Phys. Commun. **59**, 399 (1990).
- [44] see <http://www.flapw.de>
- [45] H. Krakauer, M. Posternak and A. J. Freeman, Phys. Rev. B **19**, 1706 (1979).
- [46] D. R. Hamann, L. F. Mattheiss and H. S. Greenside, Phys. Rev. B **24**, 6151 (1981).
- [47] E. Wimmer, H. Krakauer and A. J. Freeman, Adv. Electronics Electron Phys. **65**, 337 (1985).
- [48] In the scalar relativistic approximation (SRA) [49, 70, 71, 72] of the full relativistic Kohn–Sham equations the mass-velocity and Darwin terms are included to all orders of $(1/c^2)^n$, where c is the velocity of light, but the spin–orbit interaction is systematically omitted. In this approach the angular momentum quantum number ℓ and the spin quantum number σ remain good quantum numbers.

- [49] D. D. Koelling and B. N. Harmon, J. Phys. C (Solid State Physics) **10**, 3107 (1977).
- [50] C. Li, A. J. Freeman, H. J. F. Jansen, and C. L. Fu, Phys. Rev. B **42**, 5433 (1990).
- [51] J. M. Soler and A. R. Williams, Phys. Rev. B **42**, 9728 (1990).
- [52] R. Yu, D. Singh, and H. Krakauer, Phys. Rev. B **43**, 6411 (1991).
- [53] S. Blügel, (Forschungszentrum Jülich, Jül. Report 2197, 1988).
- [54] D. Singh, Phys. Rev. B **40**, 5428 (1989).
- [55] G. W. Fernando, Phys. Rev. B **41**, 903 (1990).
- [56] R. Wu and A. J. Freeman, Comp. Phys. Comm. **76**, 58 (1993).
- [57] D. Singh, Phys. Rev. B **43**, 6388 (1991).
- [58] E. Sjöstedt, L. Nordström, D. Singh, Solid State Commun. **114**, 15 (2004).
- [59] Ph. Kurz, F. Förster, L. Nordström, G. Bihlmayer, and S. Blügel, Phys. Rev. B **69**, 024415 (2004).
- [60] Y. Mokrousov, G. Bihlmayer, and S. Blügel, Phys. Rev. B **72**, 045402 (2005).
- [61] M. Usuda, N. Hamada, T. Kotani, and M. van Schilfgaarde, Phys. Rev. B **66**, 125101 (2002)
- [62] M. L. Cohen, Phys. Rep. **110**, 293 (1984).
- [63] W. E. Pickett, Comp. Phys. Rep. **9**, , (1)15 (1989).
- [64] T. Takeda and J. Kübler, J. Phys. F **9**, 661 (1979).
- [65] S. Goedecker, Phys. Rev. B **47**, 9881 (1993).
- [66] J. Yu, A. J. Freeman, R. Podloucky, P. Herzig, and P. Weinberger, Phys. Rev. B **43**, 532 (1991).
- [67] W. Ning, C. Kailai, and W. Dingsheng, Phys. Rev. Lett. **56**, 2759 (1986).
- [68] J. Tersoff and D. R. Hamann, Phys. Rev. Lett. **50**, 1998 (1983).
- [69] S. Heinze, S. Blügel, R. Pascal, M. Bode, R. Wiesendanger, Phys. Rev. B **58**, 16432 (1998).
- [70] T. Takeda, Z. Physik B **43**, 32 (1978).
- [71] J. H. Wood and A. M. Boring, Phys. Rev. B **18**, 2701 (1978).
- [72] H. Gollisch and L. Fritsche, phys. stat. sol. (b) **86**, 145 (1978).
- [73] J. Korringa, Physica **13**, 392 (1947).
- [74] W. Kohn and N. Rostoker, Phys. Rev. **94**, 1111 (1954).

- [75] T. H. Dupree, *Ann. Phys. (N. Y.)*, **15**, 63 (1961); J. L. Beeby, *Proc. Roy. Soc. London Ser. A* **302**, 113 (1967); G. J. Morgan, *Proc. Phys. Soc.* **89**, 365 (1966).
- [76] For a review of the KKR method, see N. Papanikolaou, R. Zeller, and P. H. Dederichs, *J. Phys.: Condens. Matter* **14**, 2799 (2002).
- [77] R. Zeller and P. H. Dederichs, *Phys. Rev. Lett.* **42**, 1713 (1979).
- [78] R. Zeller, P. H. Dederichs, B. Újfalussy, L. Szunyogh, and P. Weinberger, *Phys. Rev. B* **52**, 8807 (1995); K. Wildberger, R. Zeller, and P. H. Dederichs *Phys. Rev. B* **55**, 10074 (1997).
- [79] Ph. Mavropoulos, N. Papanikolaou, and P. H. Dederichs *Phys. Rev. B* **69**, 125104 (2004).
- [80] M. Asato, A. Settels, T. Hoshino, T. Asada, S. Blügel, R. Zeller, and P. H. Dederichs *Phys. Rev. B* **60**, 5202 (1999).
- [81] I. Galanakis, G. Bihlmayer, V. Bellini, N. Papanikolaou, R. Zeller, S. Bluegel, and P.H. Dederichs, *Europhys. Lett.* **58**, 751 (2002).
- [82] M. Freyss, N. Papanikolaou, V. Bellini, R. Zeller, and P. H. Dederichs *Phys. Rev. B* **66**, 014445 (2002).
- [83] B. Nonas, K. Wildberger, R. Zeller, P. H. Dederichs, and B. L. Gyorffy *Phys. Rev. B* **57**, 84 (1998)
- [84] H. Ebert and S. Mankovsky, *Phys. Rev. Lett.* **90**, 077404 (2003).
- [85] N. Papanikolaou, J. Opitz, P. Zahn, and I. Mertig *Phys. Rev. B* **66**, 165441 (2002).
- [86] V. Popescu, H. Ebert, B. Nonas, and P. H. Dederichs *Phys. Rev. B* **64**, 184407 (2001)
- [87] S. Lounis, Ph. Mavropoulos, P. H. Dederichs, S. Blügel, *Phys. Rev. B* **72**, 224437 (2005).
- [88] R. Zeller, *J. Phys. C* **20**, 2347 (1987).
- [89] J. Kudrnovský, V. Drchal, I. Turek, and P. Weinberger, *Phys. Rev. B* **50**, 16105 (1994).